Chemical Engineering Journal 475 (2023) 146474

Contents lists available at ScienceDirect

Chemical Engineering Journal

journal homepage: www.elsevier.com/locate/cej

The self-adjuvant heterocyclic lipid nanoparticles encapsulated with vaccine and STAT3 siRNA boost cancer immunotherapy through DLN-targeted and STING pathway

Zixu Liu [a], Qingqing Wang [a], Yupeng Feng [a], Linxuan Zhao [b], Nan Dong [a], Yu Zhang [a], Tian Yin [c], Haibing He [a], Xing Tang [a,*], Jingxin Gou [a,*], Li Yang [a,*]

[a] Department of Pharmaceutics Science, Shenyang Pharmaceutical University, Wenhua Road 103, Shenyang, China
[b] Department of Pharmaceutics, Jilin University, Xinmin Street 1163, Changchun, China
[c] Department of Functional Food and Wine, Shenyang Pharmaceutical University, Wenhua Road 103, Shenyang, China

ARTICLE INFO

Keywords:
Heterocyclic Lipid Nanoparticles
Cancer Vaccine
STAT3 siRNA
Draining Lymph Node
STING pathway
Tumor immunosuppressive microenvironment

ABSTRACT

A great potential of tumor vaccine-based immunotherapy has been emerged; however, the low cross-presentation of tumor antigens, intrinsic immunosuppressive signaling of dendritic cells (DCs) and the immunosuppression in tumor microenvironment (TME) hindered the progress of tumor vaccine. In this article, approaches employed heterocyclic lipid nanoparticles (LNP) as a tumor vaccine and signal transduction and activator of transcription 3 (STAT3) siRNA carrier as well as a "self-adjuvant" by targeting draining lymph node (DLN) and stimulating stimulator of interferon genes (STING)-mediated type I interferon (IFN) innate immune response were proposed. Model antigens ovalbumin peptide 257–264 (OVA) were cross-presented to activate T cells; STAT3 siRNA acted synergistically with OVA to improve DCs maturation, enhance antigen presentation and abrogate immunosuppressive TME; heterocyclic lipids induced the production of type I IFN via activating the STING pathway. Compared to DLin-MC3-DMA LNP, heterocyclic LNPs, especially A18-LNP, targeted DLN, delivered much OVA and STAT3 siRNA into cytoplasm of antigen-presenting cells (APCs, mainly DCs), activated STING pathway, promoted DCs maturation and antigen presentation, abrogated immunosuppression in TME, therefore, leading to robust anti-cancer response. Thus, heterocyclic LNPs efficiently delivered tumor vaccine and STAT3 siRNA and simultaneously activated the immune system through DLN-targeted and STING pathway, provided better anti-tumor effects, suggesting a promising strategy for cancer immunotherapy.

1. Introduction

Cancer is a major public health problem worldwide [1], current treatments include surgery, radiotherapy, chemotherapy, and immunotherapy [2]. With the outbreak of COVID-19, vaccines are getting more and more attention [3,4]. The purpose of anti-tumor vaccines is to enhance cell-mediated immune responses, such as typical T lymphocyte responses, to remove or reduce tumor cells without harming normal cells [5]. Dendritic cells (DCs) initiate effector T cells to fight tumors and play a crucial role in tumor vaccines [6]. Vaccines also can be used in combination with other oncology therapies, such as immune agonists and checkpoint inhibitors, as well as RNA therapeutics [7]. RNA-based therapies can not only modulate gene expression, but also modulate proteins or antigens that provoke an immune response to treat a variety of disease types including infectious diseases, cancer, immune and genetic diseases [8]. siRNA can knock down the expression of target genes in a sequence-specific manner by mediating degradation of targeted mRNA [9].

However, in clinical applications, tumor vaccines have consistently exhibited relatively weak response rates and negative results, which have been attributed to low cross-presentation of tumor antigens, intrinsic immunosuppressive signaling of DCs and the immunosuppressive tumor microenvironment (TME) [10]. STAT3 is a confluence of signaling pathways for many cytokines (IL-6, IL-10, IL-11, etc.), growth factors (vascular endothelial growth factor (VEGF), fibroblast growth factor (FGF), etc.) and some proto-oncogenes (K-Ras, cAbl, Src, etc.) [11]. The activation of STAT3 is transient and rapid in normal physiological conditions. However, the persistent activation and high

* Corresponding authors.
E-mail addresses: tanglab@126.com (X. Tang), jxgou_syphu@163.com (J. Gou), yangli@syphu.edu.cn (L. Yang).

https://doi.org/10.1016/j.cej.2023.146474
Received 21 August 2023; Accepted 4 October 2023
Available online 5 October 2023

expression of STAT3 is appeared in many tumors, including melanoma, colonel cancer and so on, leading to the progress of tumors [12–15]. Activated STAT3 signaling induces upregulation of the expression of some proto-oncogenes (c-Myc, etc.) and anti-apoptotic genes (Bcl-2, Bcl-XL, etc.), leading to inhibited apoptosis and sustained cell proliferation [16]. In addition, aberrantly activated STAT3 can induce the expression of matrix metalloproteinases (MMPs) to promote tumor metastasis and invasion [17]. Activated STAT3 also up-regulates tumor immunosuppressive cells (regulatory T cells (Tregs), myeloid-derived suppressor cells (MDSCs)) and down-regulates pro-inflammatory cytokines to promote tumor immune escape [18]. Furthermore, STAT3 is not only involved in DCs growth and development, but also inhibits DCs activation and maturation, and triggers aberrant differentiation into tolerant DCs, thereby promoting immune tolerance [19–21]. Deleting STAT3 gene not only suppress growth and induce apoptosis of tumor cells, but also improve antigen-presenting ability, promote DCs maturation, abrogate immunosuppressive TME and enhance antitumor T cell immunity [22,23]. Therefore, STAT3 siRNA was combined with anti-tumor vaccine.

The delivery efficiency of tumor vaccine to antigen-presenting cells (APCs, mainly DCs) has some deficiencies [24]. Meanwhile, RNA is difficult to enter cells to play effect, due to the anionic charge, ease of degradation by RNases and large molecular weight [25]. The mainstream carrier delivery system, lipid nanoparticle (LNP), relatively easily absorbed by APCs. In 2018, FDA approved Onpattro, the first LNP-based siRNA therapy [26]. Moderna, CureVac and BioNTech's COVID-19 vaccines all use LNP delivery technology [27,28]. Thus, we proposed to prepare LNP to encapsulate STAT3 siRNA and model antigens ovalbumin peptide 257–264 (OVA). LNP is composed of ionizable lipids, cholesterol, membrane skeleton, polyethylene glycol (PEG) lipids [27,29]. However, elevated cytokine levels and increased immunogenicity have been shown due to the repeated administration some of the ionizable lipids containing LNP [29]. Besides, some vaccine still contained lipopolysaccharide (LPS) or toll-like receptors (TLR) agonist as an adjuvant, induce local and systemic inflammation [30]. Furthermore, LNP accumulates in the liver, so most current LNP delivery systems are liver-targeted, and the issue of effective delivery to extra-hepatic organs needs to be addressed [31,32]. Cationic lipids are a very important component of RNA delivery. To solve the current problems of LNP, a new cationic lipid-like material, which has the ability to balance the maturation and activation of antigen-specific immune cells while avoiding toxicity due to systemic activation of the immune system, and

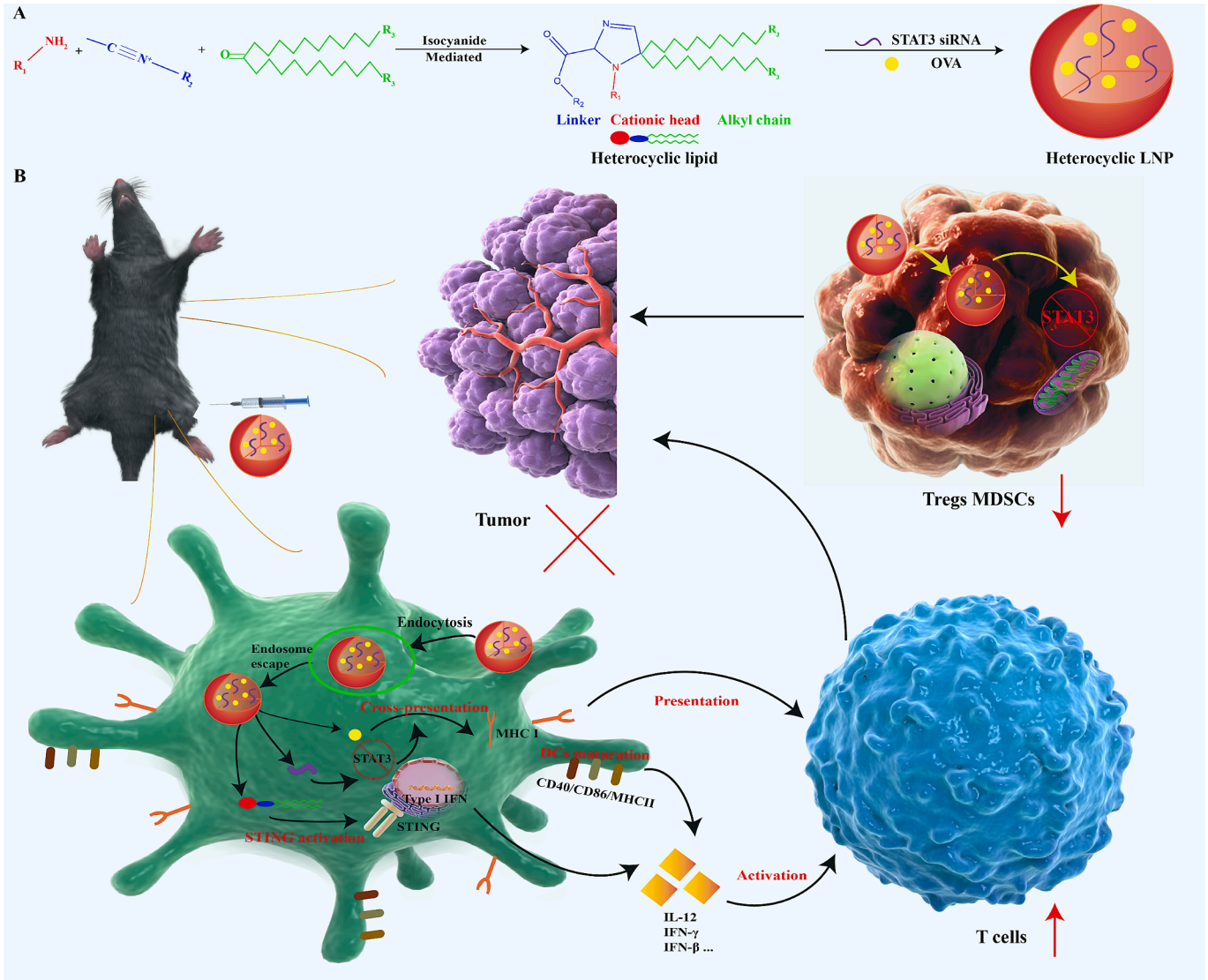

Scheme 1. (A) The heterocyclic lipids were designed and synthesized. And heterocyclic LNPs encapsulated with model antigens OVA and STAT3 siRNA were formulated. (B) The schematic representation of enhanced cancer immunotherapy in heterocyclic LNPs, including DLN-targeted, promoted DCs maturation, improved antigen cross-presentation, abrogated immunosuppressive TME and activated STING pathway.

deliver to extra-hepatic organs (especially draining lymph node (DLN)/ DCs), should be developed.

Here, approaches employed heterocyclic LNPs as the STAT3 siRNA and vaccine carrier as well as a "self-adjuvant" by targeting DLN and stimulating stimulator of interferon genes (STING)-mediated type I interferon (IFN) innate immune response were proposed (Scheme 1). Heterocyclic lipids with cyclic amino head groups were synthesized, then heterocyclic LNPs were formulated and encapsulated with OVA and STAT3 siRNA (Scheme 1A). After subcutaneous injection, heterocyclic LNPs targeted DLN, and A18-LNP had the best DLN-targeted ability. The heterocyclic LNPs delivered OVA and STAT3 siRNA into cytoplasm of APCs (mainly DCs) via improved endocytosis, and enhanced endo/ lysosome escape effect. The major histocompatibility complex (MHC) class I presented the released OVA to activate T cells to play typical T lymphocyte responses. The released STAT3 siRNA acted synergistically with OVA to promote the maturation of DCs, advance the presentation of antigen, abrogate immunosuppression and enhance anti-tumor immunity, while heterocyclic lipids in the cytoplasm induces the production of type I IFN via activating the STING pathway, which also promotes activation of T cells. The integration of promoted DCs maturation, enhanced antigen cross-presentation, abrogated immunosuppression and STING activation can boost cancer immunotherapy (Scheme 1B). Heterocyclic LNPs efficiently delivered cancer vaccine and STAT3 siRNA and simultaneously activated the immune system through DLN-targeted and STING pathway, provided better antitumor effects.

2. Materials and methods

2.1. Materials

N-(3-Aminopropyl) pyrrolidine (A2), Ethyl isocyanoacetate (Iso), OVA were provided by Macklin (Shanghai, China). 9,26-Pentatriacontadien-18-one (2DC18) was from Pfaltz & Bauer. 3-(2-ethyl-1-piperidinyl)-1-propanamine (A18) was from Santa Cruz Biotechnology, Inc. Advanced Vehicle Technology Co., Ltd (Shanghai, China) supplied (6Z,9Z,28Z,31Z)-heptatriacont-6,9,28,31-tetraene-19-yl 4-(dimethylamino) butanoate (DLin-MC3-DMA), 1,2-dimyristoyl-*rac*-glycero-3-methoxypolyethylene glycol-2000 (DMG-PEG_{2000}), 1,2-distearoyl-*sn*-glycero-3-phosphocholine (DSPC) and cholesterol. Negative control siRNA (Nc siRNA), STAT3 siRNA, CY5/FAM -STAT3 siRNA were provided by Genepharma (Shanghai, China). Xian ruixi Biological Technology Co., Ltd provided CY3/7-OVA. RiboGreen® RNA Quantitation Kit, mouse interleukin 6 (IL-6) ELISA Kit, interleukin 1 beta (IL-1β) ELISA Kit, interferon γ (IFN-γ) ELISA Kit, tumor necrosis factor-α (TNF-α) ELISA Kit, Micro BCA protein assay kit were purchased from ThermoFisher Scientific. Recombinant Murine Interleukin 4 (IL-4) and Granulocyte-Macrophage Colony Stimulating Factor (GM-CSF) were from Beyotime (Shanghai, China). Cell Counting Kit-8 (CCK-8), Lyso-Tracker Red DND-99, Carboxyfluorescein diacetate, succinimidyl ester (CFSE) and 4′,6-Diamidino-2-phenylindole dihydrochloride (DAPI) were from Dalian Meilun Biotechnology Co., Ltd. Elabscience Biotechnology provided fluorochrome-labeled anti-mouse monoclonal antibodies (FITC anti-mouse CD11c, FITC anti-mouse CD4, APC anti-mouse CD86, APC anti-mouse CD8a, APC anti-mouse CD11b, APC anti-mouse MHCII, PE anti-mouse CD40, PE anti-mouse Gr-1, PE anti-mouse CD3) and interleukin 12 (IL-12) ELISA Kit, interferon β (IFN-β) ELISA Kit. Anti-STAT3 Rabbit pAb, anti-FOXP3 Rabbit pAb, anti-IRF-3 Rabbit pAb, anti-Actin Mouse mAb, anti-CD8 Rabbit mAb, iF488-Tyramide and TUNELE assay kit, HPR/Cy3 conjugated Goat Anti-Rabbit IgG were provided by Servicebio (Wuhan, China). Mouse OVA-specific immunoglobulin G (sIgG) ELISA Kit was from Sspbio (Wuhan, China). Shenyang Pharmaceutical University provided B16F10 cells, $DC_{2.4}$ cells, and $RAW_{264.7}$ cells. Meisen CTCC (Zhejiang, China) provided the OVA-transfected B16 melanoma cell line (B16-OVA). Shenyang Pharmaceutical University Animal Center provided 6–8 weeks C57BL/6 mice; all procedures gained approval from the Animal Ethics Committee of Shenyang Pharmaceutical University.

2.2. LNPs synthesis and formulation optimization

According to previous study [33], heterocyclic lipids were synthesized by mixing amines, ketones and isocyanides. In briefly, A2 or A18, Iso, and 2DC18 (1:1:1, molar ratio) in dichloromethane and ethanol was stirred at room temperature for 24 h. The structure was confirmed by H^1-NMR (Fig.S1). The molar ratios of lipid fractions, the weight ratio of total lipid to antigen, and the weight ratio of total lipid to siRNA were optimized.

A model LNP, DLin-MC3-DMA LNP was prepared and hereinafter referred to as LNP. For LNP, DLin-MC3-DMA: DSPC: Cholesterol: DMG-PEG_{2000} (45: 10: 43.5: 1.5, mM) was dissolved in ethanol, OVA and STAT3 siRNA (total lipid: siRNA: OVA 30:1:3, w) (N/P 6) were dissolved in 20 mM sodium acetate buffer (pH 5.0). For A2/A18-LNP, the ratio of A2/A18-Iso-2DC18: DSPC: Cholesterol: DMG-PEG_{2000} was 50: 10: 37.5: 2.5 and the ratio of total lipid: siRNA: OVA was 10:1:3 (N/P 3). Ethanol and aqueous phases were mixed in a microfluidic device at a ratio of 1:3 (v). LNP, A2-LNP and A18-LNP (LNPs) were dialyzed with 1X PBS at 4 °C for 1 h.

2.3. The characterization of LNPs

ZetaSizer (Nano-ZS ZEN3700, Malvern, UK) was used to evaluate the particle size and ζ-potential of LNPs, and LNPs were diluted with PBS. Transmission electron microscope (TEM) was used to observe the morphology of LNPs, and LNPs were stained with phosphotungstic acid [34]. According to instructions, the encapsulation efficiency of siRNA was studied using RiboGreen® RNA Quantitation Kit, Micro BCA protein assay kit was used to study the encapsulation efficiency of OVA. B16F10 cells and DC2.4 cells were added to 12-well plates at a concentration of 2×10^5cells/well and incubated overnight. The flow cytometer (BD FACSAria^{TM} III) was used to measure the fluorescence intensity of FAM, after transfection with LNPs@FAM-STAT3 siRNA (50 nM) for 16 h.

2.4. In vitro capture of tumor cell lysates

B16F10 cells were lysed by the freeze–thaw method and the supernatant was obtained by centrifugation. The lysate concentration was determined by BCA method. Blank preparations were mixed with cell lysates in different weight ratio (1:1, volume). ZetaSizer was used to evaluate the size and ζ-potential of blank LNPs-B16F10 tumor cell lysate complex.

2.5. In vitro release of siRNA

siRNA release was measured using a gel retention assay. The high concentration LNPs were diluted 10-fold in PBS (pH 7.4 and pH 5.0) to mimic the extracellular and intracellular environments, respectively. The diluted LNPs were incubated at 37 °C. The supernatant was removed by ultracentrifugation at predetermined time points, and agarose gel electrophoresis was used to determine the release of siRNA.

2.6. The cytoplasmic delivery of LNPs

Firstly, CCK-8 method was used to evaluate the cytotoxicity effect of LNPs to immune cells ($DC_{2.4}$ cells and $RAW_{264.7}$ cells) and tumor cells (B16F10 cells) [2]. The cellular uptake of LNPs was studied in DCs. $DC_{2.4}$ cells (3×10^5 cells/well) were incubated with CY3-OVA (2 μg/mL) and FAM-STAT3 siRNA (50 nM) for 2 h and 4 h. The flow cytometer was used to measure the fluorescence intensity of FAM and CY3 in $DC_{2.4}$ cells. The cellular uptake of LNPs at 0.5, 1, 2, and 4 h was also visualized by confocal laser scanning microscope (CLSM, LEICA, Germany). The lysosomal escape effect of LNPs was also studied in $DC_{2.4}$ cells. Lyso-Tracker Red DND-99 (75 nM) was added to stain cells for 1 h, after

incubation with LNPs@FAM-STAT3 siRNA for 4 h. CLSM was used to observe the images, after fixed with 4% paraformaldehyde and stained with DAPI solution.

2.7. Dcs maturation assay

Bone marrow-derived DCs (BMDCs) were acquired as protocol described [35]. In brief, bone marrow cells washed from C57BL/6 mice femurs were cultured in RPMI 1640 medium with 10% FBS, 10 ng/mL IL-4 and 20 ng/mL GM-CSF. Half of the culture medium was changed every 2 days. On day 6, immature BMDCs were collected. BMDCs or $DC_{2.4}$ cells were incubated with PBS, blank LNPs, LNPs, Nc siRNA/OVA, and STAT3 siRNA/OVA (2 μg/mL OVA, 50 nM siRNA). After 24 h incubation, the cells were stained with FITC anti-mouse CD11c, APC anti-mouse MHCII, and PE anti-mouse CD40 at 4 ℃ for 1 h. The flow cytometer was used to measure % $MHCII^+$ in $CD11c^+$ cells and % $CD40^+$ in $CD11c^+$ cells. Meanwhile, the IL-6, IL-12, IFN-γ, IFN-β, IL-1β and TNF-α contents in the supernatant of BMDCs were determined using ELISA Kits, according to the instructions.

2.8. The expression of STAT3 and IFNB1/IRF-3 in BMDCs

BMDCs were incubated with PBS, STAT3 siRNA/OVA, and LNPs (2 μg/mL OVA, 50 nM siRNA) for 24 h or 72 h. Servicebio®RT First Strand cDNA Synthesis Kit was used to generate cDNA. The following primers: *STAT3* (mouse, NM_010510.1), *ifnb1* (mouse, NM_011486.5) were used. And Bio-rad CFX RT-PCR detection system was used to detect the expression of mRNA. The mRNA level of *STAT3* and *ifnb1* were calculated and normalized with *GAPDH* mRNA. Furthermore, SDS-PAGE was used to separate the samples, after the total protein of BMDCs was extracted [36]. Anti-IRF-3 and anti-STAT3 antibody were used for western blotting analysis, and the loading control was Actin.

2.9. The antigen presentation of LNPs

As previous described, we acquired the splenocytes of C57BL/6 mice [36]. In briefly, fresh mouse spleens were obtained and digested with collagenase (ThermoFisher Scientific), then the red blood cells were removed with red blood cells lysis buffer (Dalian Meilun Biotechnology Co., Ltd). After 24 h incubation with LNPs, splenocytes were stained with PE anti-mouse H-2 Kb bound to SIINFEKL antibody (ThermoFisher Scientific) for 2 h at 4 ℃. The flow cytometer was used to measure the fluorescence intensity of PE in splenocytes.

2.10. In vivo antigen capture and biodistribution of LNPs

To evaluate antigen capture and delivery *in vivo*, experiments were conducted using cy7-OVA. C57BL/6 mice were administrated subcutaneously (s.c.) with 40 μg/mouse free cy7-OVA, and then injected with PBS or blank LNPs at the same location immediately 5 min later. After 6 h, an *in vivo* imaging system (IVIS Lumina III, PerkinElmer, USA) was used to image the distribution of cy7-OVA and the isolated DLN. Meanwhile, biodistribution of cargoes was also evaluated. C57BL/6 mice were injected s.c. with 1 nmol/mouse cy5-STAT3 siRNA and 40 μg/mouse cy7-OVA. After 12 and 24 h administration, IVIS was also used to image the distribution of cy7-OVA and cy5-STAT3 siRNA *in vivo*. Meanwhile, DLN was isolated to image the distribution of cargoes. Furthermore, DLN was also sectioned at 10 μm and the sections were stained with DAPI for visualization.

2.11. The immunization therapy of LNPs

6–8 weeks C57BL/6J mice were injected s.c. with B16-OVA cells (10^6 cells/mouse). The tumor volume was approximately 50 mm^3 on day 6. The mice were divided into six groups, and injected s.c. with PBS, Nc siRNA/OVA, STAT3 siRNA/OVA, LNP, A2-LNP and A18-LNP, respectively. The mice were administrated with 40 μg/mouse OVA and 1 nmol/mouse siRNA every 5 days for three doses. Every 2–3 days, the body weight and tumor size were measured, and tumor volume was calculated: tumor volume (mm^3) = (length × width × width)/2. The levels of OVA-specific IgG, IL-12, IFN-γ and IFN-β in serum were measured. After the mice were sacrificed, the tumors of mice were collected and weighed. RT-qPCR assay was also subjected to determine the mRNA expression of *STAT3* and *IFNb1* in tumors of mice. Furthermore, TUNEL staining was used to evaluate the apoptosis of tumors, and image-pro software was used to calculate the apoptotic cells.

2.12. In vivo cells recruitment

The tumors and spleens were removed, four days after the last immunization. The tumor or spleen cell suspensions were incubated with PE anti-mouse CD3, APC anti-mouse CD8a, and FITC anti-mouse CD4 at 4 ℃ for 1 h. The flow cytometer was used to measure the % $CD8^+CD3^+$ cells and % $CD4^+CD3^+$ cells. The cell suspensions were also labeled with APC anti-mouse CD86 and FITC anti-mouse CD11c to identify mature DCs. The tumor cell suspensions were also stained with PE anti-mouse Gr-1 and APC anti-mouse CD11b to identify MDSCs. DLNs of mice were also removed and the cell suspensions were labeled with APC anti-mouse CD86 and PE anti-mouse CD40 to identify mature DCs, the % $CD86^+CD40^+$ cells were measured by the flow cytometer. Moreover, the spleens were fixed for CD8 immunohistochemical analysis, and the tumors were immunofluorescent stained with FOXP3 and CD8, and confocal microscopy was used to record the images [36].

2.13. Safety evaluation

Plasma was collected before the mice were sacrificed to conduct the biochemical analysis, including liver function test and renal function test. Furthermore, after the mice were sacrificed, the tumors and major organs were obtained for hematoxylin and eosin (H&E) staining [37].

2.14. In vivo cytotoxic T lymphocyte (CTL) assay

Four days after the second immunization, splenocytes were collected. Half of the splenocytes were pulsed with SIINFEKL peptide at 37 °C for 2 h. The unpulsed and peptide-pulsed cells were labeled with 0.05 μM or 0.5 μM CFSE, respectively. Equal numbers of $CFSE_{low}$ and $CFSE_{high}$ cells were mixed together and injected intravenously into the immunized mice [38]. After 18 h, splenocytes were collected and subjected to flow cytometry analysis.

2.15. Statistical analysis

The mean value ± SD was used to present all data. The one-way analysis of variance (ANOVA) test and Student's *t* test were used to evaluate the statistical analysis of data. When $P < 0.05$, there was a statistically significant difference.

3. Results and discussion

3.1. The preparation and characterization of LNPs

Firstly, an ionizable lipid-like material as the basis of heterocyclic LNPs was synthesized (Fig. 1). The structure consists of an alkyl ketone lipid tail, an isocyanide linker, and an amine head group. The heterocyclic lipid A2/A18-Iso-2DC18 share several structural similarities: (1) the absence of hydroxyl groups; (2) two amines in the polar head group spaced by three carbons; and (3) the presence of at least one tertiary amine [33]. DLin-MC3-DMA is the only ionizable lipids approved currently for siRNA therapies [39], so we choose DLin-MC3-DMA as the control ionizable lipid. The molar ratios of lipid fractions, the weight ratio of total lipid to antigen, and the weight ratio of total lipid to siRNA

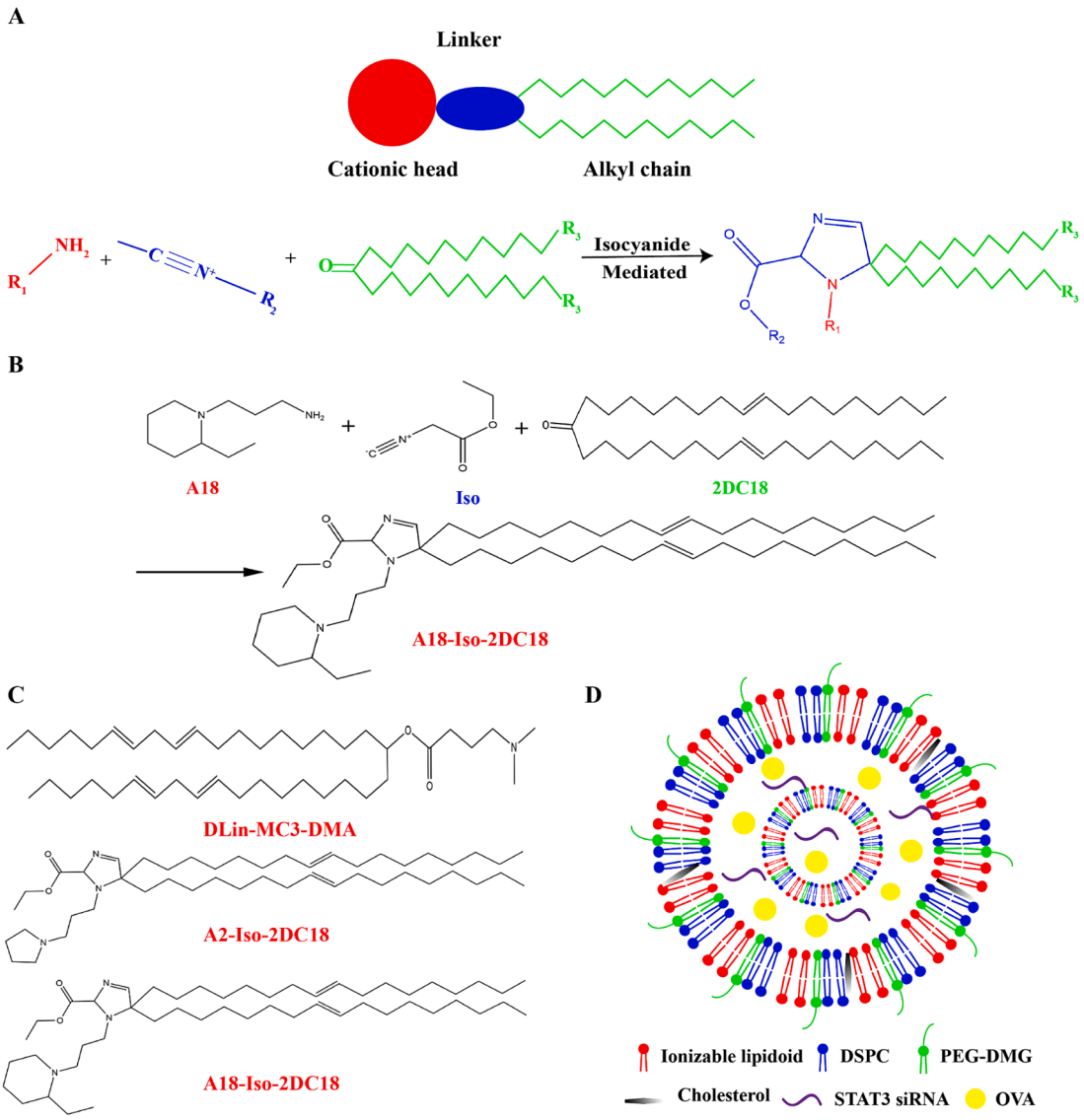

Fig 1. (A) Proposed reaction mechanisms of the isocyanide mediated reaction. (B) The synthesis of A18-Iso-2DC18. (C) The structure of ionizable lipids. (D) Schematic of LNPs.

influence on the transfection efficiency, morphology, encapsulation efficiency, and particle size of LNPs [40]. According to the particle size, for LNP, the molar ratios of DLin-MC3-DMA: DSPC: Choleaterol:DMG-PEG_{2000} was 45: 10: 43.5: 1.5, and for A2/A18-LNP, the molar ratios of A2/A18-Iso-2DC18: DSPC: Choleaterol:DMG-PEG_{2000} was 50: 10: 37.5: 2.5 (Fig.S2). Ionizable lipids efficiently encapsulate RNA and OVA, interact with cell membranes and promote endosome escape; DSPC improves lipid bilayer stability, aids membrane fusion and endosome escape; DMG-PEG prolongs body circulation via reducing particle binding to plasma proteins *in vivo*; cholesterol regulates membrane fluidity and improves stability. The weight ratio of total lipid to antigen was studied by B16F10 tumor cell lysate *in vitro* capture assay. With the B16F10 tumor cell lysate weight ratio increased, the size of the blank LNPs-B16F10 tumor cell lysate complex significantly increased. In addition, the zeta potential of blank LNPs-B16F10 tumor cell lysate complex decreased from positive to negative charge. For LNP, the weight ratio of total lipid to antigen was 10:1, for A2/A18-LNP, it was 10:3, indicating heterocyclic lipid can capture more antigen *in vitro* (Fig. 2A). According to transfection efficiency, for LNP, the weight ratio of total lipid: STAT3 siRNA: OVA was 30:1:3 (N/P 6), for A2/A18-LNP, it was 10:1:3 (N/P 3) (Table S1, 2).

LNP with hydrodynamic size at 115.3 ± 1.34 nm and ζ-potential at 16.9 ± 3.76 mV, A2-LNP with hydrodynamic size at 107.9 ± 1.57 nm and ζ-potential at 7.41 ± 3.20 mV, A18-LNP with hydrodynamic size at 124.4 ± 3.45 nm and ζ-potential at 7.80 ± 4.40 mV were prepared (Table 1, Fig. 2B, C). A morphology that was roughly spherical was observed, under the TEM images (Fig. 2D). The OVA and siRNA were distributed in the inner water phase of LNPs (Fig. 1D), and OVA and STAT3 siRNA had an encapsulation efficiency of over 95% (Table 1). At pH 7.4, LNP released partial siRNA at 6 h, A2-LNP and A18-LNP hardly released siRNA, demonstrating that heterocyclic LNPs have more stable encapsulation ability. At pH 5.0, LNPs were rapidly released, demonstrating that LNPs were pH-responsive nanoparticles (Fig. 2E). The positively charged lipids can interact with ionized endosomal membranes to promote membrane fusion and destabilization in the acidic endosomal microenvironment, leading to the release of siRNA and OVA from LNPs and endosomes to function in the cytoplasm. At physiological pH, ionizable lipids remain neutral, improving stability and reducing systemic toxicity. The particle size of LNPs remained almost unchanged during 30 days at 4 ℃, indicating the stability of LNPs (Fig. 2F).

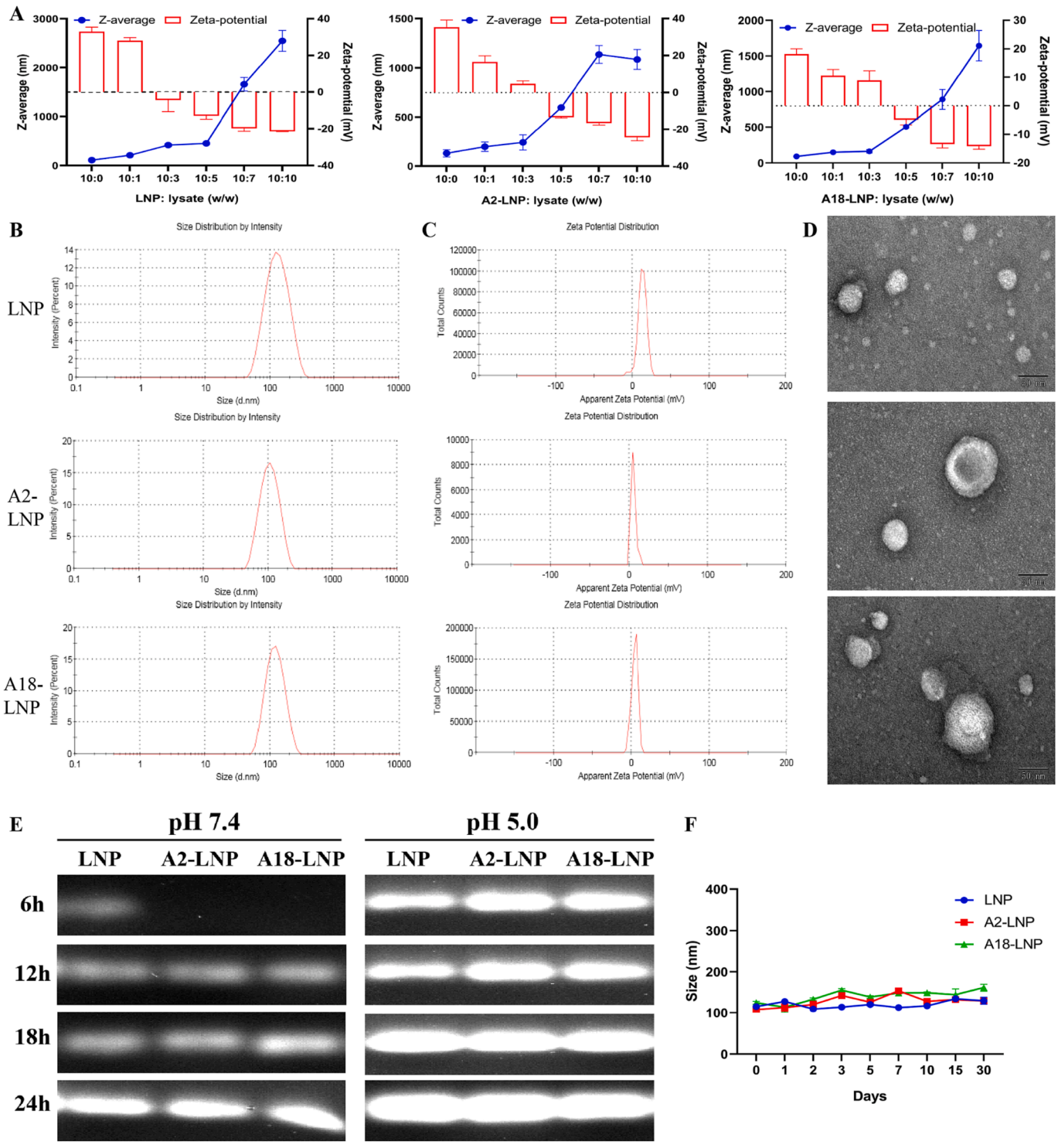

Fig 2. (A) The particle size and zeta potential of blank LNPs-B16F10 tumor cell lysate complex (n = 3). The (B) particle size, (C) zeta potential, and (D) TEM images of LNPs (scale bars: 50 nm). (E) The release of LNPs in PBS (pH 7.4 and pH 5.0) was evaluated by agarose gel. (F) The particle size of LNPs over 30 days at 4 ℃ (n = 3).

3.2. The cytoplasm delivery by LNPs

Firstly, the cytotoxicity of blank LNPs and LNPs were evaluated in $DC_{2.4}$ cells, $RAW_{264.7}$ cells and B16F10 cells. No significant cytotoxicity was observed after incubation in $DC_{2.4}$ cells and $RAW_{264.7}$ cells, indicating the safety of LNPs (Fig. 3A, C). No significant cytotoxicity was observed after incubation in B16F10 cells with STAT3 siRNA/OVA and blank LNPs. However, a significant cytotoxicity was observed after incubation in B16F10 cells with LNPs (Fig. 3B). Thus, LNPs inhibited proliferation of tumor cells and had an excellent biocompatibility with immune cells.

DCs are the most functional and specialized antigen-presenting cells in the body [41]. The STAT3 siRNA and antigen need to enter the cytoplasm of DCs for effective action. Compared to free solution, a significantly higher fluorescent intensity of FAM and CY3 was shown in LNPs. And the fluorescent intensity of A2/18-LNP was higher than that

Table 1
Physical properties of LNPs.

	LNP	A2-LNP	A18-LNP
Z-average (nm)	115.3 ± 1.34	107.9 ± 1.57	124.4 ± 3.45
PDI	0.167 ± 0.006	0.118 ± 0.005	0.115 ± 0.006
Number Mean (nm)	69.65 ± 2.28	65.60 ± 2.30	81.90 ± 4.23
Zeta potential (mV)	16.9 ± 3.76	7.41 ± 3.20	7.80 ± 4.40
Encapsulation Efficiency of siRNA	101.45%	97.18%	99.23%
Encapsulation Efficiency of OVA	95.10%	95.80%	96.86%

of LNP, there was a significantly difference between the A18-LNP group and LNP group (Fig. 3E). The CLSM results showed that free solution was rarely able to enter the cells. Compared to free solution group, a higher cellular uptake was shown, and the fluorescent intensity upregulated with time in all LNPs groups. Moreover, the heterocyclic LNPs had a better uptake, while the uptake of A18-LNP was slightly stronger than that of A2-LNP (Fig. 3D and Fig.S3). The heterocyclic LNPs were better able to deliver cargoes into DCs, especially A18-LNP had the best ability. LNPs entered the endosome after taken up by the cells. The STAT3 siRNA and OVA tended to inactivate, due to the acidic environment in endosome. The green signal (STAT3 siRNA) in the free solution was very low, indicating free solution was difficult to enter the cells. STAT3 siRNA of all LNPs groups was distributed throughout the cytoplasm and could escape from the red-labeled endosomes/lysosomes. Moreover, heterocyclic LNPs had the stronger endo/lysosomal escape effect, especially A18-LNP had the strongest endo/lysosomal escape effect (Fig. 3F). When LNPs were taken up by cells, lipids were ionized and positively charged under endosomal pH conditions (pH 5–6), and the positively charged lipids readily fused with the endosomal-lysosomal membrane, allowing LNPs to escape to the cytosol, dissociated and released STAT3 siRNA and OVA. Heterocyclic lipids have two amines in the head group, which may interact more strongly with the cell membrane and further promote endosomal escape. Thus, heterocyclic LNPs could better deliver STAT3 siRNA and OVA into cytoplasm of DCs.

3.3. *Heterocyclic LNPs promote DCs maturation, STING activation, and antigen presentation*

To evaluate the gene silencing effect of LNPs encapsulated STAT3 siRNA, RT-PCR and WB assay were studied. The expression of *STAT3* mRNA (Fig. 5A) and STAT3 (Fig. 5E-H, Fig.S4 and Fig.S5) were significantly lower in all LNPs groups, compared with the solution group. The expression of *STAT3* mRNA and STAT3 in the A18-LNP group was 0.42-fold and 0.58-fold lower than that in the LNP group. Meanwhile, the STAT3 expression in BMDCs was time-dependence, as the incubation time increasing, the expression was decreased. These indicated that heterocyclic LNPs could better silence *STAT3* gene, mainly due to cytoplasm delivery of heterocyclic LNPs.

Compared with the Nc siRNA/OVA group, the STAT3 siRNA/OVA group upregulated the expression of CD40 and MHCII in $DC_{2.4}$ cells (Fig. 4A-C) and BMDCs (Fig. 4D-F), and improved the secretion of IL-12, IL-6, IL-1β, IFN-γ and TNF-α (Fig. 4G), confirming that STAT3 siRNA restored DCs dysfunction and promoted DCs maturation, consistent with previous findings [22,42]. STAT3 is abbreviately activated in immune cells. Immune cells play an important role in preventing tumorigenesis via detecting and removing abnormally transformed cancer cells. However, persistent activation of STAT3 in these immune cells activates the expression of downstream genes IL-6, IL-10 and VEGF, which proliferate hematopoietic stem cells (HPC). Then HPCs produced many cytokines, which activated STAT3 in plasmacytoid dendritic cells (pDCs) and immature myeloid cells (IMCs) [43]. The maturation of DCs was blocked due to the sustained expression of IL-10 in IMCs. Meanwhile, pDCs improved the aggregation of Tregs, and STAT3 was able to up-regulate the transcription of FOXP3, a transcription factor that is closely related to tumorigenesis, which further inhibited the maturation of DCs [44,45]. Mature DCs can effectively activate initial T cells and enhance the body's anti-tumor immune response. These suggest that sustained activation of STAT3 can inhibit DCs function. Thus, stronger DCs maturation can be exerted when combine STAT3 siRNA with OVA. In the blank preparations, the secretion of cytokines and the expression of CD40 and MHCII were slightly increased in the blank A2-LNP and A18-LNP groups, compare to blank LNP group, indicating that heterocyclic lipids could slightly induce DCs maturation (Fig. 4C, F, G). Compared to the solution group, the secretion of cytokines and the expression of CD40 and MHCII were significantly upregulated in LNPs groups, particularly in the heterocyclic LNPs groups. And there was a significant difference between the A18-LNP group and LNP group, indicating that the heterocyclic LNPs groups had better DCs maturation, with A18-LNP having the strongest DCs maturation capability (Fig. 4A-G). Heterocyclic LNPs delivered much OVA and STAT3 siRNA into the cytoplasm of DCs to promote DCs maturation, in addition, the unique structural features of heterocyclic lipid may promote DCs maturation by activating the STING pathway.

Recently, the STING signaling pathway has emerged as a toll-like receptors/retinoic acid-inducible gene-I-like receptors (TLR/RLR)-independent mediator of the host innate immune response [46]. STING is considered as a central regulator of innate and adaptive immunity. When stimulated, STING induces type I IFN, the expression of cytokines and T-cell recruitment factors leads to activate DCs and tumor-specific T cells, significantly enhances tumor antigen-specific immune responses [47,48]. The activated STING conformation changes and further activates downstream TANK-binding kinases 1 (TBK1) and the transcription factor interferon regulatory factor 3 (IRF3), inducing the production of type I IFN [47]. The *ifnb1* genes were the main genes associated with STING activation, and their expression leads to high secretion of type I IFN and pro-inflammatory cytokines [49]. The enhanced STING activation by heterocyclic LNPs was evaluated, the expression of *ifnb1* mRNA and IRF-3 were measured. The expression of *ifnb1* mRNA in the heterocyclic LNPs groups was significantly higher than that in the LNP group, with the A18-LNP group being 3.3 times higher than the LNP group, suggesting that heterocyclic LNPs can promote *ifnb1* mRNA expression (Fig. 5B). The expression of IRF-3 in the heterocyclic LNPs groups was significantly higher than that in the LNP group, with the A18-LNP group being 1.27 times higher than the LNP group, indicating heterocyclic LNPs can promote IRF-3 expression (Fig. 5C, D and Fig.S4). Meanwhile, only heterocyclic LNPs groups significantly increased the secretion of IFN-β (Fig. 4H), and the secretion of pro-inflammatory cytokines were also higher than that of other groups (Fig. 4G). These indicated heterocyclic lipids can activate the STING pathway. The cyclic lipid head groups could bind with STING C-terminal domain binding pocket, typically shared by the natural ligand c[G(2′,5′)pA(3′,5′)p] (Protein Data Bank (PDB): 4EF4, 4KSY) and the small molecule DMXAA (PDB: 4QXP). For PDB 4KSY, the dissociation constant (*K*d) of A18 was 19.26 μM, and the *K*d of A2 was 24.98 μM [33]. Thus, heterocyclic lipids can activate the STING pathway.

The antigen is delivered to the cytoplasm of the APCs, where it can be degraded by the proteasome and incorporated into MHC class I molecules for cross-presentation to cytotoxic $CD8^+$ T cells [49,50]. The antibodies (H-2 Kb bound to SIINFEKL) react with the OVA-derived peptide SIINFEKL bound to H-2 Kb of MHC class I. The antibodies have proven to be very useful tracking the quantity of these specific APCs. The antibodies were used to assess the antigen presentation ability. Compared with Nc siRNA/OVA, the expression of SIINFEKL-bound MHC I was improved in STAT3 siRNA/OVA, indicating STAT3 siRNA can improve antigen-presenting ability (Fig. 5I). Meanwhile, the expression was increased in all LNPs groups. Moreover, heterocyclic LNPs groups had a higher expression, indicating heterocyclic lipids promoted powerful antigen presentation. These maybe due to more antigen was delivered into the cytoplasm of APCs in heterocyclic LNPs.

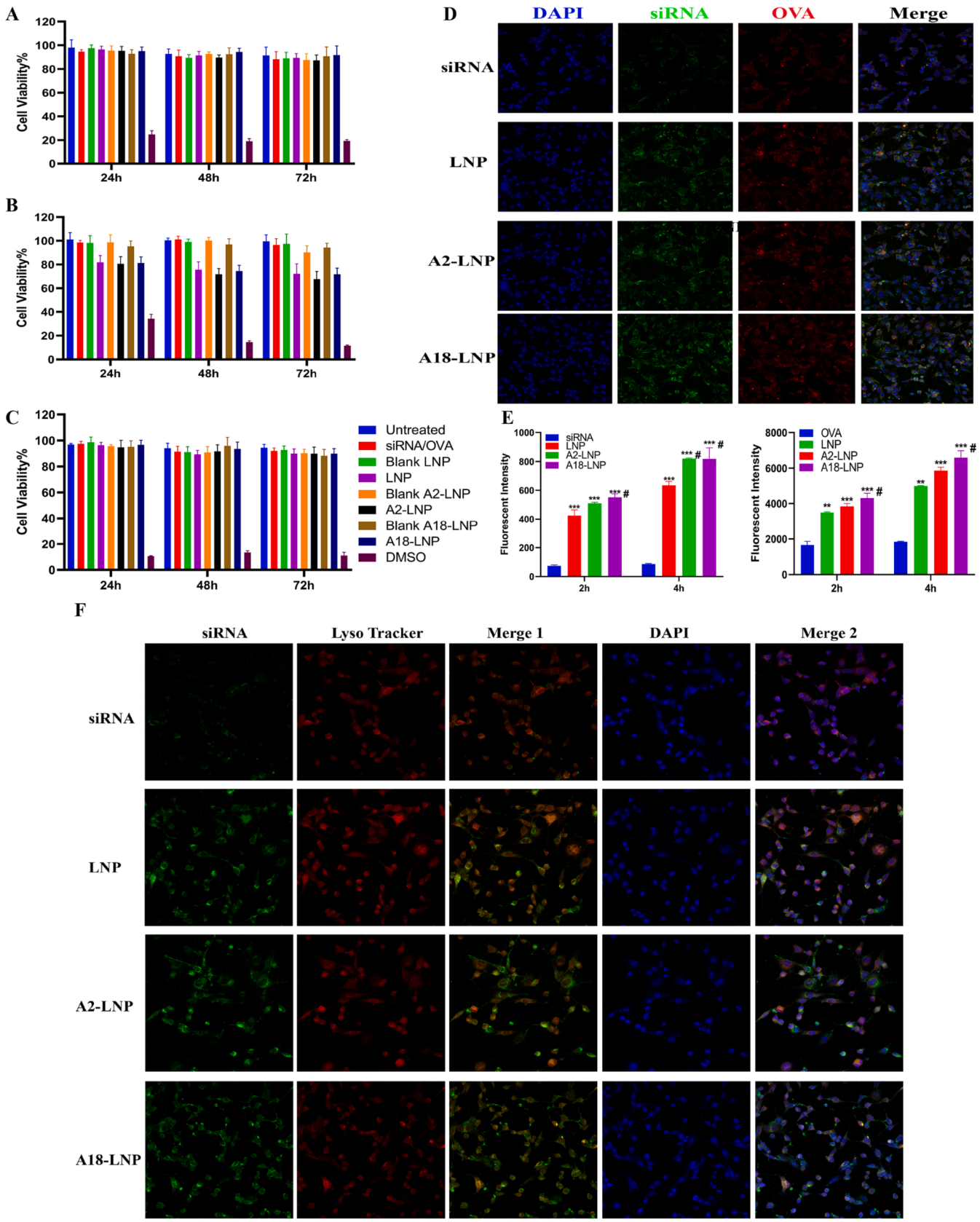

Fig 3. The cell viability of blank LNPs and LNPs on (A) $DC_{2.4}$ cells, (B) B16F10 cells and (C) $RAW_{264.7}$ cells (n = 6). (D) CLSM observed the images of $DC_{2.4}$ cells after 4 h incubation (×200). (E) The fluorescence intensity of $DC_{2.4}$ cells after 2 and 4 h incubation (n = 3). * vs STAT3 siRNA/OVA, # vs LNP. (F) Escape of internalized siRNA from the lysosomes of $DC_{2.4}$ cells (×200).

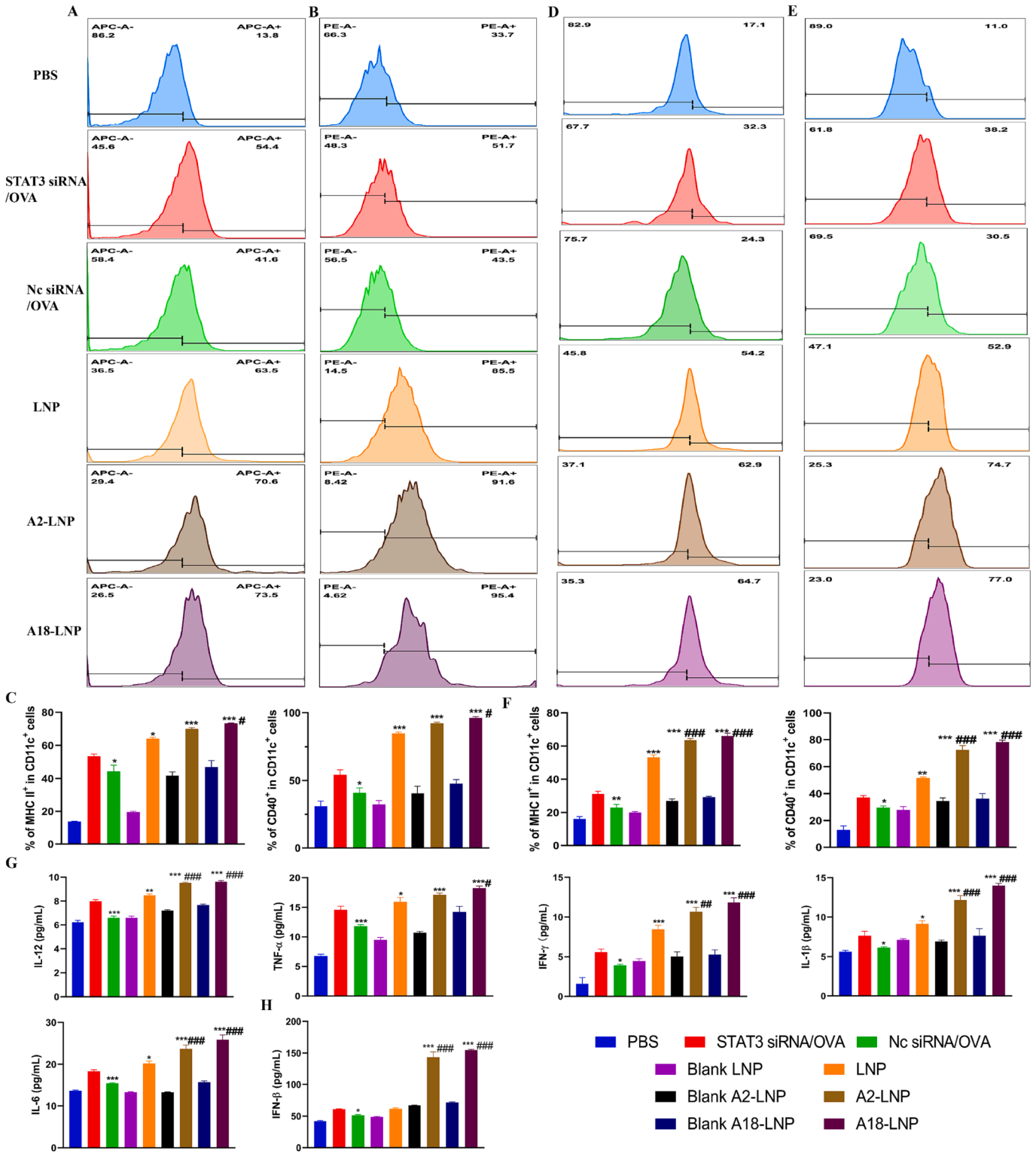

Fig 4. The expression of (A) APC-MHCII and (B) PE-CD40 in $DC_{2.4}$ cells. (C) Quantification of $MHCII^+$ and $CD40^+$ (n = 3). The expression of (D) APC-MHCII and (E) PE-CD40 in BMDCs. (F) Quantification of $MHCII^+$ and $CD40^+$ (n = 3). The content of (G) TNF-α, IFN-γ, IL-6, IL-12, IL-1β, and (H) IFN-β in BMDCs (n = 3). $DC_{2.4}$ cells and BMDCs were incubated with 2 μg/mL OVA and 50 nM siRNA for 24 h. * vs STAT3 siRNA/OVA, # vs LNP.

3.4. Heterocyclic LNPs promote DLN-targeted

Firstly, we studied the administration method on the effect of DLN-targeted. After 6 h subcutaneous injection, the fluorescence intensity of cy7-OVA and cy5-STAT3 siRNA in DLN was significantly higher than other administrations (Fig.S6). The route of administration has a great influence on the absorption of DLN, in which the nanocarriers are enriched in the tissue mesenchyme after interstitial administration, and are more likely to enter the lymphatic vessels due to the characteristics of large interstitial spaces between lymphatic endothelial cells and the lack of basement membrane. Interstitial administration injected antigens can be captured by APCs such as DCs residing in peripheral tissues,

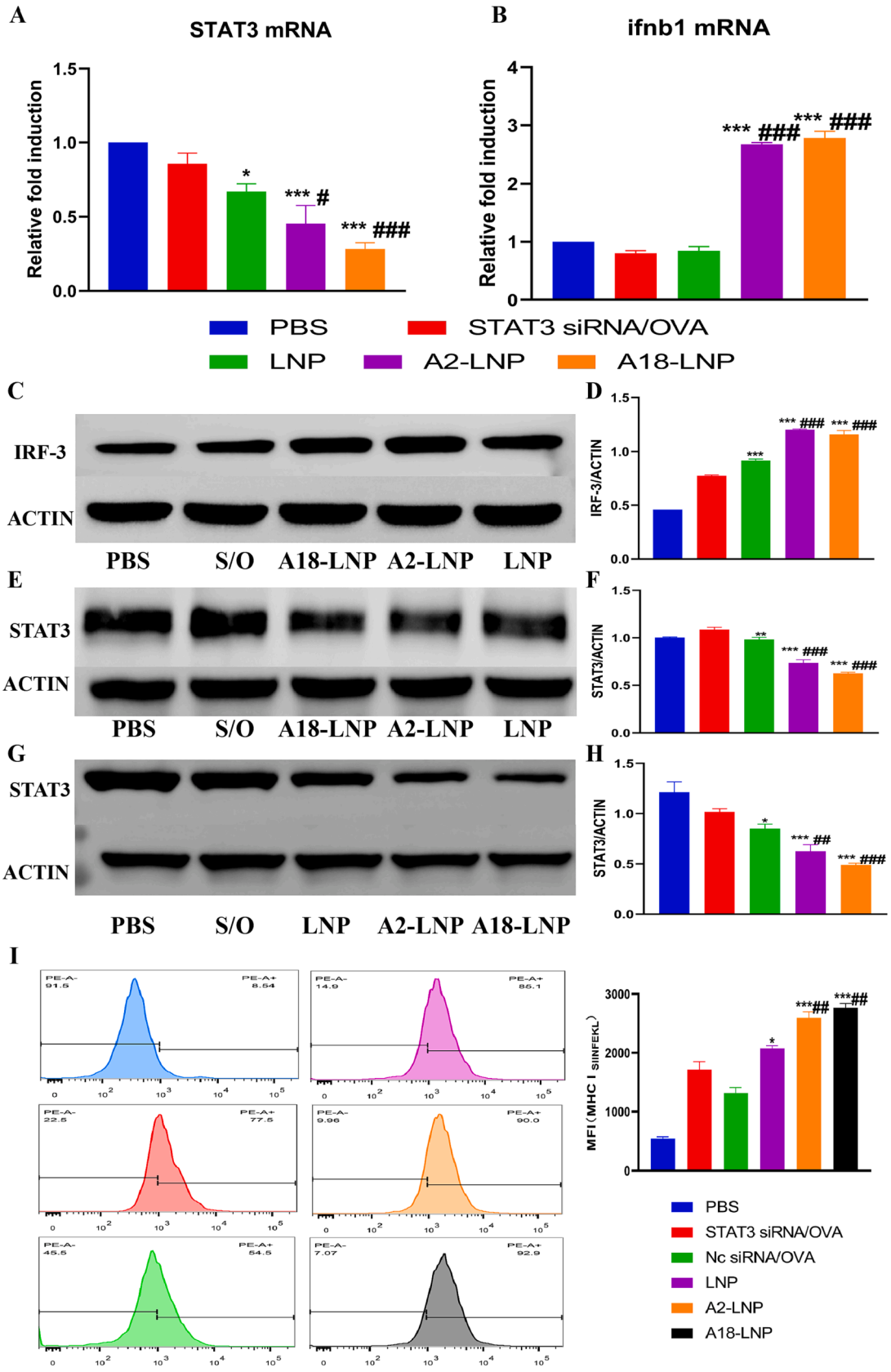

Fig 5. Relative fold induction of (A) *STAT3* and (B) *ifnb1* genes (n = 3). The expression of (C) IRF-3 and (E) STAT3 in BMDCs for 24 h. The (D) IRF-3/ACTIN and (F) STAT3/ACTIN was quantified (n = 3). (G) The expression of STAT3 in BMDCs for 72 h. (H) Quantification of STAT3/ACTIN (n = 3). (I) The expression and MFI of MHC I $_{SIINFEKL}$ on splenocytes for 24 h (n = 3). BMDCs and splenocytes were incubated with 2 μg/mL OVA and 50 nM siRNA. * vs STAT3 siRNA/OVA, $^{\#}$ vs LNP.

which are then digested and rendered as MHC. Then activated MHC-expressing APCs will cross the lymphatic endothelium from the interstitium and enter the lymphatic vessels through the interstitial fluid. Subcutaneous has high tissue interstitial pressure and higher lymphatic flow rate, so the DLN absorption efficiency is the highest after subcutaneous administration [51,52]. Thus, LNPs were administered by subcutaneous injection.

Besides, antigen capture and delivery to DLN *in vivo* was evaluated, fluorescence intensity in DLN was significantly higher in mice treated with free cy7-OVA followed by injection of blank LNPs than followed by injection of PBS. Especially, the fluorescence intensity in DLN of blank heterocyclic LNPs were much higher, the blank A18-LNP group was 69.61 times of PBS group, and was 11.41 times of blank LNP group, demonstrating heterocyclic LNPs can capture free antigen and deliver them to DLN (Fig. 6A). We expect heterocyclic LNPs to similarly capture tumor associated antigens and presences them to APCs in DLN, enhancing antitumor effect and reducing the immune escape. The biodistribution was also studied, heterocyclic LNPs delivered cargoes into DLN (Fig. 6B, C and Fig.S7). At 12 h, the CY7-OVA fluorescence intensity in DLN of the A18-LNP group was 37.96 folds of solution group, and was 6.08 folds of LNP group, the CY5-STAT3 siRNA fluorescence intensity was 56.14 folds of solution group, and was 11.85 folds of LNP group. The distribution in the deep of DLN was also evaluated. The red fluorescence intensity in heterocyclic LNPs was higher than LNP and the intensity of A18-LNP group was highest (Fig. 6D, E). Surface charge is critical for nanoparticle priming into the DLN. The tissue interstitium contains a large amount of negatively charged glycosaminoglycans, so neutral and negatively charged nanoparticles are more likely to drain from the interstitium into the lymphatic vessels [53]. The zeta potential of heterocyclic LNPs was close to neutral, more likely to be delivered to DLN. The retention of positively charged particles in the interstitium increases, forming a "reservoir" in the subcutis, where the particles slowly enter the lymphatic vessels or are taken up by APCs in the interstitium and enter the lymphatic vessels. Furthermore, DLN contains a large number of DCs, when nanoparticles are taken up by DCs, they can enter the lymphatic vessels with DCs [54–56]. Compared to the LNP, the heterocyclic LNPs had a better uptake by DCs, leading to enter DLN. Thus, heterocyclic LNPs promote DLN-targeted.

3.5. Heterocyclic LNPs induce robust anti-cancer response

The tumor of STAT3 siRNA/OVA group was reduced, compared to the Nc siRNA/OVA group, demonstrating combination of OVA and STAT3 siRNA showed better anti-tumor effect. The tumor of LNPs groups was significantly decreased, especially heterocyclic LNPs groups, compared with STAT3 siRNA/OVA group. There was significantly difference between the LNP and heterocyclic LNPs, and A18-LNP had the lowest tumor volume and weight (Fig. 7A, C, E). Remarkably, dramatic apoptosis in tumor tissues of heterocyclic LNPs was elicited (Fig. 7G, H and Fig.S8). Heterocyclic LNPs promoted the secretion of IL-12 and IFN-γ to induce the CTL response (Fig. 7D). Meanwhile, free OVA solution showed very low antibody response due to its low immunogenicity. Heterocyclic LNPs showed higher antibody response, especially A18-LNP has the strongest antibody response (Fig. 7D). Heterocyclic LNPs also induced the mRNA expression of *ifnb1* and increased the secretion of IFN-β, demonstrating activate the STING pathway *in vivo* (Fig. 7D, F). Heterocyclic LNPs, especially A18-LNP, reduced the *STAT3* mRNA expression in tumors, demonstrating heterocyclic LNPs could effectively silence STAT3 gene *in vivo* (Fig. 7F). Compared to the PBS group, the body weight of all administrated groups was no significantly difference, demonstrating the biosafety of LNPs (Fig. 7B). A significantly extended survival rate was shown in LNPs groups, the median survival of A18-LNP group (42 day) was significantly higher than LNP group (36 day) (Fig. 7I). Thus, codelivery of STAT3 siRNA and OVA by heterocyclic LNPs, especially A18-LNP, significantly enhanced anti-cancer activity. Heterocyclic LNPs targeted DLN, delivered much OVA and STAT3 siRNA into APCs, activated STING pathway, promoted DCs maturation, improved antigen presentation, resulting a robust anti-cancer activity.

Compared to Nc siRNA/OVA group, STAT3 siRNA/OVA group showed higher $CD8^+$ and $CD4^+$ T cells, indicating STAT3 siRNA can promote the antitumor immune response of OVA (Fig. 8A-D, Fig. 9A-D). The heterocyclic LNPs groups showed the highest $CD8^+$ T cells and $CD4^+$ T cells. The tumor-infiltrating $CD8^+$ T cells in A18-LNP group increased by 9.57-fold than PBS group. And there was a significantly difference between the A18-LNP group and the LNP group, showing heterocyclic LNPs had better anti-cancer immune response (Fig. 8D). Moreover, active $CD8^+$ T cell infiltration was observed in the spleens and tumors of heterocyclic LNPs groups, especially A18-LNP group showed the best effect, suggesting heterocyclic LNPs can induce a robust immune response (Fig. 8I and Fig.S9, 10).

The maturation of DCs in tumors, spleens, even DLNs were also identified. Tumor associated DCs (TADC) are usually immature and dysfunctional. Compared to the Nc siRNA/OVA group, the STAT3 siRNA/OVA group elevated the expression of CD86, demonstrating the combination therapy can promote DCs maturation *in vivo* (Fig. 8E, G). The proportion of maturated TADC in heterocyclic LNPs groups was increased, the $CD86^+CD11c^+$ cells in A18-LNP group increased by 6.06-fold than PBS group (Fig. 8E, G). The proportion of maturated spleen associated DCs was also increased in heterocyclic LNPs groups (Fig. 9E, F, I). DLN is the main site where the vaccine produces its effects, the maturated DCs in DLN was also identified. Compared to Nc siRNA/OVA, STAT3 siRNA/OVA elevated the expression of CD40 and CD86, the $CD86^+CD40^+$ cells increased by 1.72-fold than Nc siRNA/OVA group. The maturated DCs in DLN of heterocyclic LNPs groups was also significantly increased, the $CD86^+CD40^+$ cells in A18-LNP group increased by 10.47-fold than PBS group, indicating heterocyclic LNPs further promoted DCs maturation by targeting DLN (Fig. 9G, J).

Treg and MDSC play an important effect in tumor progression and tumor immune escape. We identified the proportion of MDSC in tumors. The $Gr\text{-}1^+CD11b^+$ cells in STAT3 siRNA/OVA group was lower than that in Nc siRNA/OVA group, indicating deletion of *STAT3* gene was essential to overcome immunosuppression in TME. Furthermore, heterocyclic LNPs reduced the proportion of MDSC, and heterocyclic LNPs and LNP had a significant difference (Fig. 8F, H). Moreover, the heterocyclic LNPs groups down-regulated the expression of FOXP3 in tumors, especially A18-LNP had the best down-regulation effect, indicating that heterocyclic LNPs can abrogate immunosuppressive TME (Fig. 8I and Fig.S10).

OVA-specific CTL response *in vivo* was evaluated. The OVA-specific $CD8^+$ T cell could specifically kill the group of splenocytes pulsed with SIINFEKL peptide (higher fluorescence) but not the unpulsed group of splenocytes (lower fluorescence). The mice immunized with STAT3 siRNA/OVA and Nc siRNA/OVA showed less than 20% efficiency in lysing SIINFEKL-pulsed splenocytes, LNP did increase the cell lysing capability (still lower than 50%). The mice immunized with heterocyclic LNPs showed significant OVA-specific CTL response (Fig. 9H, K), in parallel with robust IFN-γ secretion (Fig. 7D). The OVA-specific killing of A18-LNP was 16-fold than that of PBS. These results showed that the heterocyclic LNPs, especially A18-LNP enables the efficient $CD8^+$ T cell activation. In summary, heterocyclic LNPs, especially A18-LNP, effectively promoted DCs maturation, reduced immunosuppressive cells (Tregs and MDSCs), further upregulated $CD4^+$ and $CD8^+$ T cells, and facilitated the establishment of anti-tumor immune response.

The biosafety was also assessed, there was no significant difference (Fig.S11A, B). And there was no significant organ damage (Fig.S11C). Nuclear pyknosis, chromatin shrinkage and many cavities were identified in tumor tissues of LNPs groups, indicating an improved antitumor effect. In brief, heterocyclic lipids can be used for safe and efficacious anti-tumor immunity.

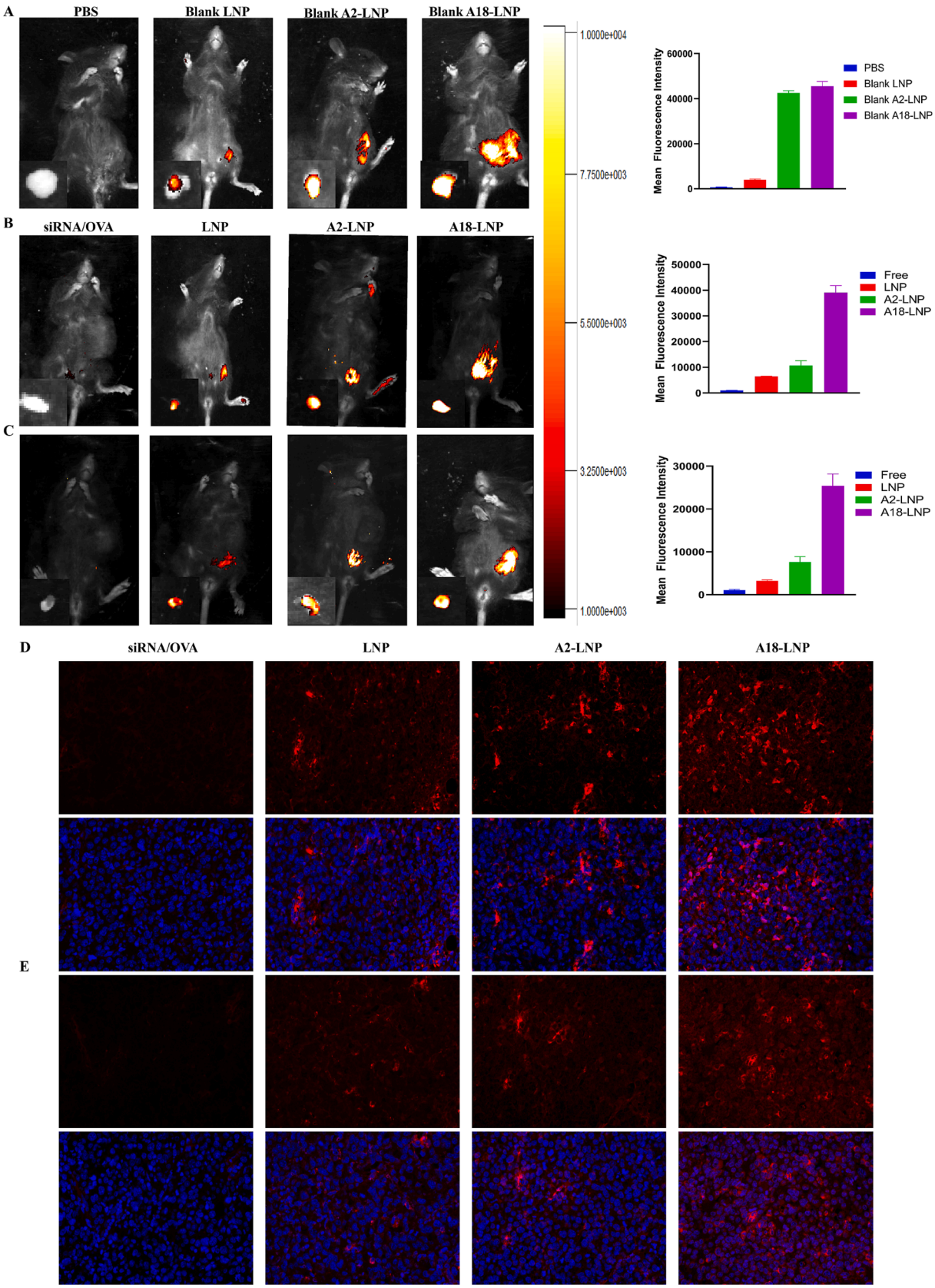

Fig 6. (A) Enhanced delivery of CY7-OVA to DLNs after being captured by blank heterocyclic LNPs *in vivo*. The CY7-OVA fluorescence image of DLN at (B) 12 h and (C) 24 h. Bruker MI SE software was used to assess the semi-quantitatively analysis of fluorescence intensity in DLNs (n = 3). The CY7-OVA (red) fluorescence image of deeper DLN at (D) 12 h and (E) 24 h (×200). The mice with B16-OVA tumor were administrated s.c. with 40 μg/mouse cy7-OVA and 1 nmol/mouse cy5-STAT3 siRNA. (For interpretation of the references to colour in this figure legend, the reader is referred to the web version of this article.)

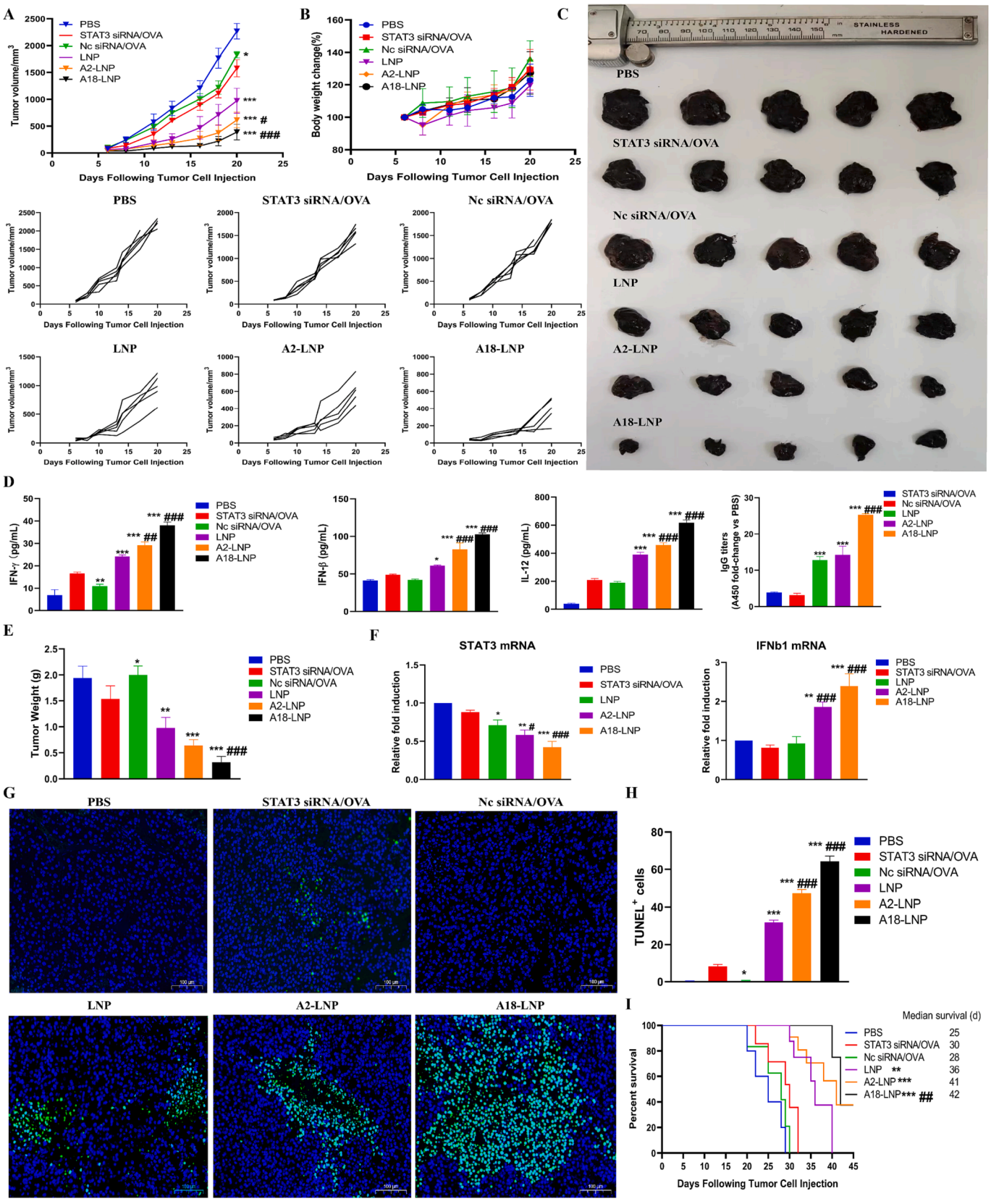

Fig 7. The (A) tumor volume, (B) body weight change, and (C) tumor images of different treatments (n = 5). (D) The secretion of OVA-sIgG, IFN-γ, IFN-β, IL-12 in serum (n = 3). (E) The tumor weight (n = 5). (F) Relative fold induction of *STAT3* and *ifnb1* genes in tumors (n = 3). (G) Cell apoptosis in tumors was detected using TUNEL assay, and (H) quantified the percentage of apoptotic cells (n = 3) (×200). (I) The survival curve of mice (n = 5). The mice with B16-OVA tumor were administrated s.c. with 40 μg/mouse OVA and 1 nmol/mouse siRNA every 5 days for three doses. * vs STAT3 siRNA/OVA, # vs LNP.

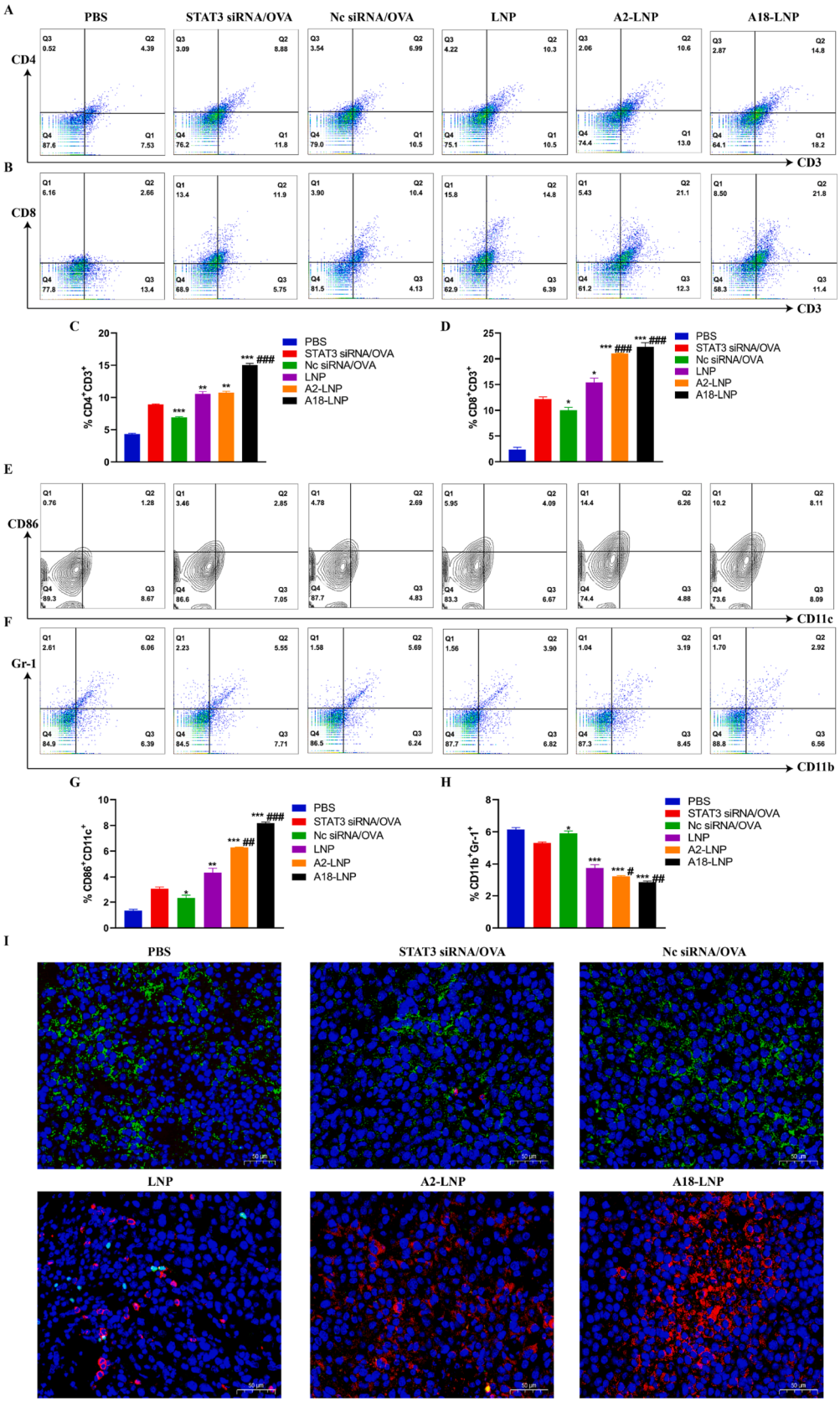

Fig 8. The tumor-infiltrating (A) $CD4^+$ and (B) $CD8^+$ T cells. Quantification of (C) $CD4^+$ and (D) $CD8^+$ T cells (n = 3). (E) The maturation of DCs in mice tumor. (F) MDSCs infiltration in tumor. (G) Quantitative results of % $CD86^+CD11c^+$ and (H) % $CD11b^+Gr\text{-}1^+$ (n = 3). (I) The immunofluorescent staining test results of CD8 (red) and FOXP3 (green) in tumors (×400). * vs STAT3 siRNA/OVA, # vs LNP. (For interpretation of the references to colour in this figure legend, the reader is referred to the web version of this article.)

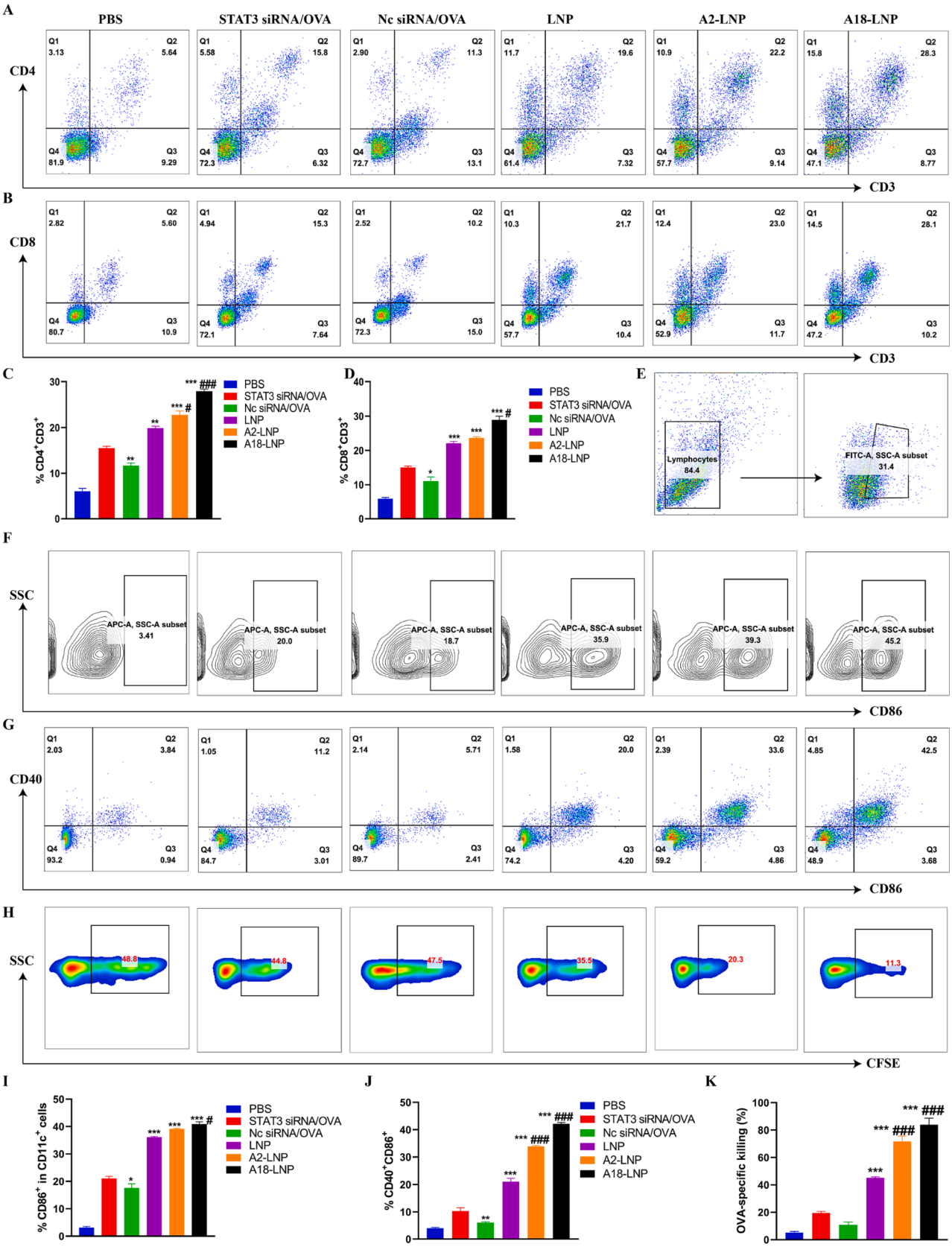

Fig 9. The spleen-infiltrating (A) $CD4^+$ and (B) $CD8^+$ T cells. Quantification of (C) $CD4^+$ and (D) $CD8^+$ T cells (n = 3). (E, F) The maturation of DCs in mice spleen. (G) The maturation of DCs in mice DLN. (H) The representative flow images of OVA-specific killing by $CD8^+$T cells in spleen. (I) Quantitative results of % $CD86^+$ in $CD11c^+$ in spleen were displayed (n = 3). (J) Quantitative results of % $CD40^+CD86^+$ in DLN (n = 3). (K) Quantitative results of OVA-specific killing (n = 2). * vs STAT3 siRNA/OVA, $^{\#}$ vs LNP.

4. Conclusion

In this study, heterocyclic LNPs were employed as a STAT3 siRNA and cancer vaccine carrier as well as a "self-adjuvant" by targeting DLN and stimulating STING-mediated type I IFN innate immune response. The OVA was cross-presented to activate T cells; the STAT3 siRNA acted synergistically with OVA to promote DCs maturation, abrogate immunosuppression, improve antigen presentation; heterocyclic lipids activated the STING pathway and induced the production of type I IFN. The integration of promoted DCs maturation, enhanced antigen cross-presentation, abrogated immunosuppression and activated STING activation can boost tumor immunotherapy. Compared to DLin-MC3-DMA LNP, heterocyclic LNPs, especially A18-LNP, targeted DLN, delivered much OVA and STAT3 siRNA into cytoplasm of DCs, activated STING pathway, promoted DCs maturation, improved antigen presentation, reduced immunosuppression in TME, thus, resulting a robust anti-cancer response. Thus, heterocyclic LNPs efficiently delivered STAT3 siRNA and cancer vaccine and simultaneously activated the immune system through DLN-targeted and STING pathway, provided better antitumor effects, suggesting a promising strategy for cancer immunotherapy.

Declaration of Competing Interest

The authors declare that they have no known competing financial interests or personal relationships that could have appeared to influence the work reported in this paper.

Data availability

Data will be made available on request.

Acknowledgment

This work was supported by Liaoning Livelihood Science and Technology Plan Joint Project (No.2021JH2/10300130) and National Key R&D Program of China (No.2020YFE0201700).

Appendix A. Supplementary data

Supplementary data to this article can be found online at https://doi.org/10.1016/j.cej.2023.146474.

References

[1] H. Sung, J. Ferlay, R. Siegel, M. Laversanne, I. Soerjomataram, A. Jemal, F. Bray, Global cancer statistics 2020: GLOBOCAN estimates of incidence and mortality worldwide for 36 cancers in 185 countries, CA: a cancer journal for clinicians 71 (3) (2021) 209–249, https://doi.org/10.3322/caac.21660.

[2] Z. Liu, L. Zhao, X. Tan, Z. Wu, N. Zhou, N. Dong, Y. Zhang, T. Yin, H. He, J. Gou, X. Tang, S. Gao, Preclinical evaluations of norcantharidin liposome and emulsion hybrid delivery system with improved encapsulation efficiency and enhanced antitumor activity, Expert Opinion on Drug Delivery 19 (4) (2022) 451–464, https://doi.org/10.1080/17425247.2022.2063834.

[3] L.R. Baden, H.M. El Sahly, B. Essink, K. Kotloff, S. Frey, R. Novak, D. Diemert, S.A. Spector, N. Rouphael, C.B. Creech, J. McGettigan, S. Khetan, N. Segall, J. Solis, A. Brosz, C. Fierro, H. Schwartz, K. Neuzil, L. Corey, P. Gilbert, H. Janes, D. Follmann, M. Marovich, J. Mascola, L. Polakowski, J. Ledgerwood, B.S. Graham, H. Bennett, R. Pajon, C. Knightly, B. Leav, W. Deng, H. Zhou, S. Han, M. Ivarsson, J. Miller, T. Zaks, C.S. Group, Efficacy and Safety of the mRNA-1273 SARS-CoV-2 Vaccine, N Engl J Med 384(5) (2021) 403-416. https://doi.org/10.1056/NEJMoa2035389.

[4] F.P. Polack, S.J. Thomas, N. Kitchin, J. Absalon, A. Gurtman, S. Lockhart, J.L. Perez, G. Perez Marc, E.D. Moreira, C. Zerbini, R. Bailey, K.A. Swanson, S. Roychoudhury, K. Koury, P. Li, W.V. Kalina, D. Cooper, R.W. Frenck, Jr., L.L. Hammitt, O. Tureci, H. Nell, A. Schaefer, S. Unal, D.B. Tresnan, S. Mather, P.R. Dormitzer, U. Sahin, K.U. Jansen, W.C. Gruber, C.C.T. Group, Safety and Efficacy of the BNT162b2 mRNA Covid-19 Vaccine, N Engl J Med 383(27) (2020) 2603-2615. https://doi.org/10.1056/NEJMoa2034577.

[5] A.J. Barbier, A.Y. Jiang, P. Zhang, R. Wooster, D.G. Anderson, The clinical progress of mRNA vaccines and immunotherapies, Nature Biotechnology 40 (6) (2022) 840–854, https://doi.org/10.1038/s41587-022-01294-2.

[6] W. Yang, G. Zhu, S. Wang, G. Yu, Z. Yang, L. Lin, Z. Zhou, Y. Liu, Y. Dai, F. Zhang, Z. Shen, Y. Liu, Z. He, J. Lau, G. Niu, D.O. Kiesewetter, S. Hu, X. Chen, In situ dendritic cell vaccine for effective cancer immunotherapy, ACS Nano 13 (3) (2019) 3083–3094, https://doi.org/10.1021/acsnano.8b08346.

[7] U. Sahin, P. Oehm, E. Derhovanessian, R. Jabulowsky, M. Vormehr, M. Gold, D. Maurus, D. Schwarck-Kokarakis, A. Kuhn, T. Omokoko, L. Kranz, M. Diken, S. Kreiter, H. Haas, S. Attig, R. Rae, K. Cuk, A. Kemmer-Brück, A. Breitkreuz, C. Tolliver, J. Caspar, J. Quinkhardt, L. Hebich, M. Stein, A. Hohberger, I. Vogler, I. Liebig, S. Renken, J. Sikorski, M. Leierer, V. Müller, H. Mitzel-Rink, M. Miederer, C. Huber, S. Grabbe, J. Utikal, A. Pinter, R. Kaufmann, J. Hassel, C. Loquai, Ö. Türeci, An RNA vaccine drives immunity in checkpoint-inhibitor-treated melanoma, Nature 585 (7823) (2020) 107–112, https://doi.org/10.1038/s41586-020-2537-9.

[8] E. Kon, U. Elia, D. Peer, Principles for designing an optimal mRNA lipid nanoparticle vaccine, Current Opinion in Biotechnology 73 (2022) 329–336, https://doi.org/10.1016/j.copbio.2021.09.016.

[9] K. Paunovska, D. Loughrey, J.E. Dahlman, Drug delivery systems for RNA therapeutics, Nature Reviews. Genetics 23 (5) (2022) 265–280, https://doi.org/10.1038/s41576-021-00439-4.

[10] Y. Chen, Y. Zhang, B. Wang, Q. Fan, Q. Yang, J. Xu, H. Dai, F. Xu, C. Wang, Blood clot scaffold loaded with liposome vaccine and siRNAs targeting PD-L1 and TIM-3 for effective DC activation and cancer immunotherapy, ACS Nano 17 (1) (2023) 760–774, https://doi.org/10.1021/acsnano.2c10797.

[11] J. Dong, X.D. Cheng, W.D. Zhang, J.J. Qin, Recent update on development of Small-Molecule STAT3 inhibitors for cancer therapy: from phosphorylation inhibition to protein degradation, Journal of Medicinal Chemistry 64 (13) (2021) 8884–8915, https://doi.org/10.1021/acs.jmedchem.1c00629.

[12] L. Lin, A. Liu, Z. Peng, H. Lin, P. Li, C. Li, J. Lin, STAT3 is necessary for proliferation and survival in colon cancer-initiating cells, Cancer research 71 (23) (2011) 7226–7237, https://doi.org/10.1158/0008-5472.Can-10-4660.

[13] Y. Guo, F. Xu, T. Lu, Z. Duan, Z. Zhang, interleukin-6 signaling pathway in targeted therapy for cancer, Cancer Treatment Reviews 38 (7) (2012) 904–910.

[14] M. Santoni, F. Massari, M. Del Re, C. Ciccarese, F. Piva, G. Principato, R. Montironi, D. Santini, R. Danesi, G. Tortora, S. Cascinu, Investigational therapies targeting signal transducer and activator of transcription 3 for the treatment of cancer, Expert opinion on investigational drugs 24 (6) (2015) 809–824, https://doi.org/10.1517/13543784.2015.1020370.

[15] V. Calò, M. Migliavacca, V. Bazan, M. Macaluso, M. Buscemi, N. Gebbia, A. Russo, STAT proteins: from normal control of cellular events to tumorigenesis, Journal of cellular physiology 197 (2) (2003) 157–168, https://doi.org/10.1002/jcp.10364.

[16] S. Rahaman, P. Harbor, O. Chernova, G. Barnett, M. Vogelbaum, S. Haque, inhibition of constitutively active Stat3 suppresses proliferation and induces apoptosis in glioblastoma multiforme cells, Oncogene 21 (55) (2002) 8404–8413, https://doi.org/10.1038/sj.onc.1206047.

[17] T. Xie, D. Wei, M. Liu, A. Gao, F. Ali-Osman, R. Sawaya, S. Huang, Stat3 activation regulates the expression of matrix metalloproteinase-2 and tumor invasion and metastasis, Oncogene 23 (20) (2004) 3550–3560, https://doi.org/10.1038/sj.onc.1207383.

[18] G. Verdeil, T. Lawrence, A.M. Schmitt-Verhulst, N. Auphan-Anezin, Targeting STAT3 and STAT5 in Tumor-Associated immune cells to improve immunotherapy, Cancers (Basel) 11 (12) (2019), https://doi.org/10.3390/cancers11121832.

[19] Y. Nefedova, M. Huang, S. Kusmartsev, R. Bhattacharya, P. Cheng, R. Salup, R. Jove, D. Gabrilovich, Hyperactivation of STAT3 is involved in abnormal differentiation of dendritic cells in cancer, Journal of Immunology 172 (1) (2004) 464–474, https://doi.org/10.4049/jimmunol.172.1.464.

[20] D. Shi, J. Yang, Q. Wang, D. Li, H. Zheng, H. Mei, W. Liu, SOCS3 ablation enhances DC-derived Th17 immune response against candida albicans by activating IL-6/STAT3 in vitro, Life Sciences 222 (2019) 183–194.

[21] J. Wang, J. Wang, W. Hong, L. Zhang, L. Song, Q. Shi, Y. Shao, G. Hao, C. Fang, Y. Qiu, L. Yang, Z. Yang, J. Wang, J. Cao, B. Yang, Q. He, Q. Weng, Optineurin modulates the maturation of dendritic cells to regulate autoimmunity through JAK2-STAT3 signaling, Nature Communications 12 (1) (2021) 6198, https://doi.org/10.1038/s41467-021-26477-4.

[22] K. Lee, T.S. Kim, Y. Seo, S.Y. Kim, H. Lee, Combined hybrid structure of siRNA tailed IVT mRNA (ChriST mRNA) for enhancing DC maturation and subsequent anticancer T cell immunity, Journal of Controlled Release 327 (2020) 225–234, https://doi.org/10.1016/j.jconrel.2020.08.009.

[23] A. Alshamsan, S. Hamdy, A. Haddadi, J. Samuel, A.O. El-Kadi, H. Uludag, A. Lavasanifar, STAT3 knockdown in B16 melanoma by siRNA lipopolyplexes induces bystander immune response In vitro and In vivo, Translational Oncology 4 (3) (2011) 178–188, https://doi.org/10.1593/tlo.11100.

[24] C. Kumar, S. Kohli, P.P. Bapsy, A.K. Vaid, M. Jain, V.S. Attili, B. Sharan, Immune modulation by dendritic-cell-based cancer vaccines, Journal of Biosciences 42 (1) (2017) 161–173, https://doi.org/10.1007/s12038-017-9665-x.

[25] C. Webb, S. Ip, N.V. Bathula, P. Popova, S.K.V. Soriano, H.H. Ly, B. Eryilmaz, V.A. Nguyen Huu, R. Broadhead, M. Rabel, I. Villamagna, S. Abraham, V. Raeesi, A. Thomas, S. Clarke, E.C. Ramsay, Y. Perrie, A.K. Blakney, Current Status and Future Perspectives on MRNA Drug Manufacturing, Mol Pharm 19(4) (2022) 1047-1058. https://doi.org/10.1021/acs.molpharmaceut.2c00010.

[26] A. Akinc, M.A. Maier, M. Manoharan, K. Fitzgerald, M. Jayaraman, S. Barros, S. Ansell, X. Du, M.J. Hope, T.D. Madden, B.L. Mui, S.C. Semple, Y.K. Tam, M. Ciufolini, D. Witzigmann, J.A. Kulkarni, R. van der Meel, P.R. Cullis, the onpattro story and the clinical translation of nanomedicines containing nucleic acid-based drugs, Nature Nanotechnology 14 (12) (2019) 1084–1087, https://doi.org/10.1038/s41565-019-0591-y.

[27] S. Ramachandran, S.R. Satapathy, T. Dutta, Delivery strategies for mRNA vaccines, Pharmaceut Med 36 (1) (2022) 11–20, https://doi.org/10.1007/s40290-021-00417-5.

[28] C. Wang, Y. Zhang, Y. Dong, Lipid Nanoparticle-mRNA formulations for therapeutic applications, Accounts of Chemical Research 54 (23) (2021) 4283–4293, https://doi.org/10.1021/acs.accounts.1c00550.
[29] L. Miao, Y. Zhang, L. Huang, mRNA vaccine for cancer immunotherapy, Molecular Cancer 20 (1) (2021) 41, https://doi.org/10.1186/s12943-021-01335-5.
[30] H. Zhang, X. You, X. Wang, L. Cui, Z. Wang, F. Xu, M. Li, Z. Yang, J. Liu, P. Huang, Y. Kang, J. Wu, X. Xia, Delivery of mRNA vaccine with a lipid-like material potentiates antitumor efficacy through toll-like receptor 4 signaling, Proceedings of the National Academy of Sciences of the United States of America 118 (6) (2021), https://doi.org/10.1073/pnas.2005191118.
[31] S. Dilliard, Q. Cheng, D. Siegwart, On the mechanism of tissue-specific mRNA delivery by selective organ targeting nanoparticles, Proceedings of the National Academy of Sciences of the United States of America 118(52) (2021). https://doi.org/10.1073/pnas.2109256118.
[32] M. Qiu, Y. Tang, J. Chen, R. Muriph, Z. Ye, C. Huang, J. Evans, E. Henske, Q. Xu, Lung-selective mRNA delivery of synthetic lipid nanoparticles for the treatment of pulmonary lymphangioleiomyomatosis, Proceedings of the National Academy of Sciences of the United States of America 119(8) (2022). https://doi.org/10.1073/pnas.2116271119.
[33] L. Miao, L. Li, Y. Huang, D. Delcassian, J. Chahal, J. Han, Y. Shi, K. Sadtler, W. Gao, J. Lin, J.C. Doloff, R. Langer, D.G. Anderson, Delivery of mRNA vaccines with heterocyclic lipids increases anti-tumor efficacy by STING-mediated immune cell activation, Nature Biotechnology 37 (10) (2019) 1174–1185, https://doi.org/10.1038/s41587-019-0247-3.
[34] Z. Liu, W. Chu, Q. Sun, L. Zhao, X. Tan, Y. Zhang, T. Yin, H. He, J. Gou, X. Tang, Micelle-contained and PEGylated hybrid liposomes of combined gemcitabine and cisplatin delivery for enhancing antitumor activity, International Journal of Pharmaceutics 602 (2021), 120619, https://doi.org/10.1016/j.ijpharm.2021.120619.
[35] M. Sauter, R.J. Sauter, H. Nording, M. Olbrich, F. Emschermann, H.F. Langer, Protocol to isolate and analyze mouse bone marrow derived dendritic cells (BMDC), STAR Protocols 3 (3) (2022), 101664.
[36] Z. Liu, L. Zhao, H. Liu, N. Dong, N. Zhou, Y. Zhang, T. Yin, H. He, J. Gou, X. Tang, L. Yang, S. Gao, Norcantharidin liposome emulsion hybrid delivery system enhances PD-1/PD-L1 immunotherapy by agonizing the non-canonical NF-kappaB pathway, International Journal of Pharmaceutics 628 (2022), 122361, https://doi.org/10.1016/j.ijpharm.2022.122361.
[37] H. Liu, Y. Kong, X. Liang, Z. Liu, X. Guo, B. Yang, T. Yin, H. He, J. Gou, Y. Zhang, X. Tang, the treatment of hepatocellular carcinoma with SP94 modified asymmetrical bilayer lipid-encapsulated cu(DDC)(2) nanoparticles facilitating cu accumulation in the tumor, Expert Opinion on Drug Delivery 20 (1) (2023) 145–158, https://doi.org/10.1080/17425247.2023.2155631.
[38] M. Luo, H. Wang, Z. Wang, H. Cai, Z. Lu, Y. Li, M. Du, G. Huang, C. Wang, X. Chen, M.R. Porembka, J. Lea, A.E. Frankel, Y.-X. Fu, Z.J. Chen, J. Gao, A STING-activating nanovaccine for cancer immunotherapy, Nature Nanotechnology 12 (7) (2017) 648–654, https://doi.org/10.1038/nnano.2017.52.
[39] F. Ferraresso, A.W. Strilchuk, L.J. Juang, L.G. Poole, J.P. Luyendyk, C.J. Kastrup, Comparison of DLin-MC3-DMA and ALC-0315 for siRNA delivery to hepatocytes and hepatic stellate cells, Molecular Pharmaceutics 19 (7) (2022) 2175–2182, https://doi.org/10.1021/acs.molpharmaceut.2c00033.
[40] S.C. Semple, A. Akinc, J. Chen, A.P. Sandhu, B.L. Mui, C.K. Cho, D.W.Y. Sah, D. Stebbing, E.J. Crosley, E. Yaworski, I.M. Hafez, J.R. Dorkin, J. Qin, K. Lam, K. G. Rajeev, K.F. Wong, L.B. Jeffs, L. Nechev, M.L. Eisenhardt, M. Jayaraman, M. Kazem, M.A. Maier, M. Srinivasulu, M.J. Weinstein, Q. Chen, R. Alvarez, S. A. Barros, S. De, S.K. Klimuk, T. Borland, V. Kosovrasti, W.L. Cantley, Y.K. Tam, M. Manoharan, M.A. Ciufolini, M.A. Tracy, A. de Fougerolles, I. MacLachlan, P. R. Cullis, T.D. Madden, M.J. Hope, Rational design of cationic lipids for siRNA delivery, Nature Biotechnology 28 (2) (2010) 172–176, https://doi.org/10.1038/nbt.1602.
[41] R. Schreiber, L. Old, M. Smyth, Cancer immunoediting: integrating immunity's roles in cancer suppression and promotion, Science (New York, N.Y.) 331(6024) (2011) 1565-70. https://doi.org/10.1126/science.1203486.
[42] Z. Luo, C. Wang, H. Yi, P. Li, H. Pan, L. Liu, L. Cai, Y. Ma, Nanovaccine loaded with poly i: C and STAT3 siRNA robustly elicits anti-tumor immune responses through modulating tumor-associated dendritic cells in vivo, Biomaterials 38 (2015) 50–60, https://doi.org/10.1016/j.biomaterials.2014.10.050.
[43] Y. Wang, Y. Shen, S. Wang, Q. Shen, X. Zhou, the role of STAT3 in leading the crosstalk between human cancers and the immune system, Cancer Letters 415 (2018) 117–128, https://doi.org/10.1016/j.canlet.2017.12.003.
[44] H. Yu, D. Pardoll, R. Jove, STATs in cancer inflammation and immunity: a leading role for STAT3, Nature Reviews Cancer 9 (11) (2009) 798–809, https://doi.org/10.1038/nrc2734.
[45] H. Yu, M. Kortylewski, D. Pardoll, Crosstalk between cancer and immune cells: role of STAT3 in the tumour microenvironment, Nature Reviews Immunology 7 (1) (2007) 41–51, https://doi.org/10.1038/nri1995.
[46] S. Iurescia, D. Fioretti, M. Rinaldi, Nucleic acid sensing machinery: Targeting innate immune system for cancer therapy, Recent Patents on Anti-Cancer Drug Discovery 13 (1) (2018) 2–17.
[47] H. Zhang, Q.D. You, X.L. Xu, Targeting stimulator of interferon genes (STING): A medicinal chemistry perspective, Journal of Medicinal Chemistry 63 (8) (2020) 3785–3816, https://doi.org/10.1021/acs.jmedchem.9b01039.
[48] G.N. Barber, STING: infection, inflammation and cancer, Nature Reviews Immunology 15 (12) (2015) 760–770, https://doi.org/10.1038/nri3921.
[49] J. Chen, M. Qiu, Z. Ye, T. Nyalile, Y. Li, Z. Glass, X. Zhao, L. Yang, J. Chen, Q. Xu, In situ cancer vaccination using lipidoid nanoparticles, Science advances 7 (19) (2021), https://doi.org/10.1126/sciadv.abf1244.
[50] M.A. Oberli, A.M. Reichmuth, J.R. Dorkin, M.J. Mitchell, O.S. Fenton, A. Jaklenec, D.G. Anderson, R. Langer, D. Blankschtein, Lipid nanoparticle assisted mRNA delivery for potent cancer immunotherapy, Nano Letters 17 (3) (2017) 1326–1335, https://doi.org/10.1021/acs.nanolett.6b03329.
[51] Y. Ding, Z. Li, A. Jaklenec, Q. Hu, Vaccine delivery systems toward lymph nodes, Advanced Drug Delivery Reviews 179 (2021), 113914.
[52] J. Chen, L. Wang, Q. Yao, R. Ling, K. Li, H. Wang, Drug concentrations in axillary lymph nodes after lymphatic chemotherapy on patients with breast cancer, Breast Cancer Research 6 (4) (2004) R474, https://doi.org/10.1186/bcr819.
[53] Z. Cheng, H. Que, L. Chen, Q. Sun, X. Wei, Nanomaterial-Based drug delivery system targeting lymph nodes, Pharmaceutics 14 (7) (2022), https://doi.org/10.3390/pharmaceutics14071372.
[54] T. Nakamura, H. Harashima, Dawn of lipid nanoparticles in lymph node targeting: Potential in cancer immunotherapy, Advanced Drug Delivery Reviews 167 (2020) 78–88.
[55] Q. Zeng, H. Jiang, T. Wang, Z. Zhang, T. Gong, X. Sun, Cationic micelle delivery of Trp2 peptide for efficient lymphatic draining and enhanced cytotoxic t-lymphocyte responses, Journal of Controlled Release 200 (2015) 1–12.
[56] N.L. Trevaskis, L.M. Kaminskas, C.J.H. Porter, From sewer to saviour — targeting the lymphatic system to promote drug exposure and activity, Nature Reviews Drug Discovery 14 (11) (2015) 781–803, https://doi.org/10.1038/nrd4608.